Cell Reports

Article

Supplementation with a high-glucose drink stimulates anti-tumor immune responses to glioblastoma via gut microbiota modulation

Graphical abstract

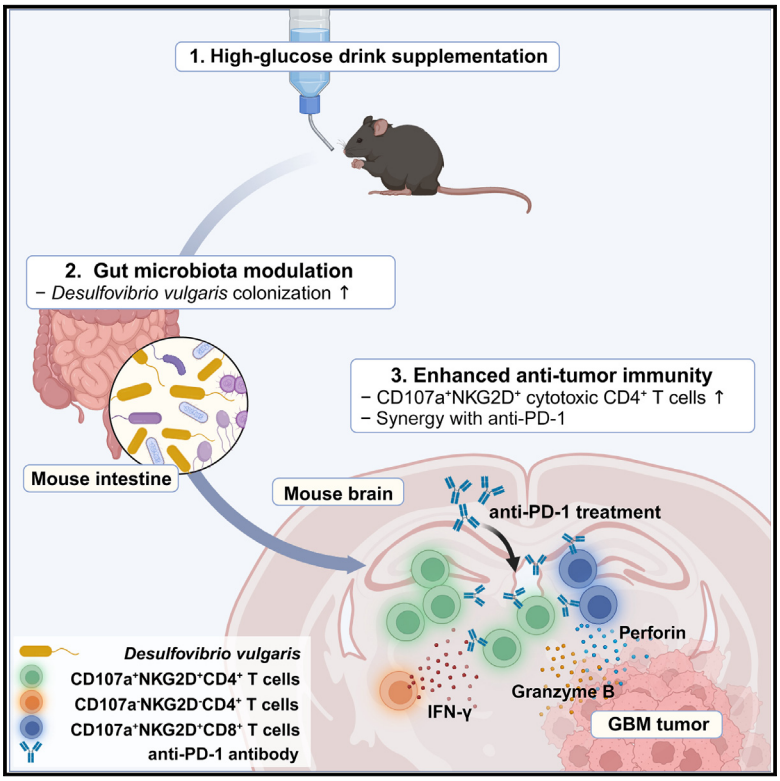

Highlights

- A high-glucose drink (HGD) increases survival rates in a glioblastoma mouse model
- HGD increased anti-tumor immunity in glioblastoma via modulation of the gut microbiota
- HGD induces gut colonization of the Desulfovibrionaceae family in GBM mice
- *Desulfovibrio vulgaris* plays a significant role in synergy with anti-PD-1

Authors

Jaeho Kim, Yumin Kim, Jeongwoo La, ..., Juhee Lim, Myoung Seung Kwon, Heung Kyu Lee

Correspondence

heungkyu.lee@kaist.ac.kr

In brief

Kim et al. report that a high-glucose drink increases survival outcomes in a glioblastoma mouse model. A high-glucose drink induces gut colonization of Desulfovibrionaceae, leading to enhanced anti-tumor immunity in the tumor microenvironment. *Desulfovibrio vulgaris* was found to have a synergistic effect with anti-PD-1 immune checkpoint blockade.

Kim et al., 2023, Cell Reports *42*, 113220
October 31, 2023
https://doi.org/10.1016/j.celrep.2023.113220

CellPress

Cell Reports

CellPress
OPEN ACCESS

Article

Supplementation with a high-glucose drink stimulates anti-tumor immune responses to glioblastoma via gut microbiota modulation

Jaeho Kim,[1] Yumin Kim,[2] Jeongwoo La,[1] Won Hyung Park,[1] Hyun-Jin Kim,[1] Sang Hee Park,[1] Keun Bon Ku,[1,3] Byeong Hoon Kang,[1] Juhee Lim,[1] Myoung Seung Kwon,[1] and Heung Kyu Lee[1,2,4,*]

[1]Graduate School of Medical Science and Engineering, Korea Advanced Institute of Science and Technology (KAIST), Daejeon 34141, Republic of Korea

[2]Department of Biological Sciences, KAIST, Daejeon 34141, Republic of Korea

[3]Department of Convergent Research of Emerging Virus Infection, Korea Research Institute of Chemical Technology, Daejeon 34114, Republic of Korea

[4]Lead contact

*Correspondence: heungkyu.lee@kaist.ac.kr

https://doi.org/10.1016/j.celrep.2023.113220

SUMMARY

A high-sugar diet induces lifestyle-associated metabolic diseases, such as obesity and diabetes, which may underlie the pro-tumor effects of a high-sugar diet. We supply GL261 syngeneic glioblastoma (GBM) mice with a short-term high-glucose drink (HGD) and find an increased survival rate with no evidence of metabolic disease. Modulation of the gut microbiota through HGD supplementation is critical for enhancing the anti-tumor immune response. Single-cell RNA sequencing shows that gut microbiota modulation by HGD supplementation increases the T cell-mediated anti-tumor immune response in GBM mice. We find that the cytotoxic $CD4^+$ T cell population in GBM is increased due to synergy with anti-programmed cell death protein 1 (anti-PD-1) immune checkpoint inhibitors, but this effect depends upon HGD supplementation. Thus, we determine that HGD supplementation enhances anti-tumor immune responses in GBM mice through gut microbiota modulation and suggest that the role of HGD supplementation in GBM should be re-examined.

INTRODUCTION

Advances in hygiene and medicine have greatly increased life expectancy in modern society, with a renewed interest in long-term health and well-being.[1] However, over the last few decades, western diets have been linked to lifestyle-associated diseases.[2] In western diets, which are characterized by low fruit and vegetable intake, high fat and salt intake, high calories, and excessive sugar, close to half the sugar may be consumed as sugar-sweetened beverages.[3,4] This excessive sugar through sweetened beverages is absorbed easily by the body, and epidemiologic studies show an association of sugar with type 2 diabetes mellitus (DM), obesity-associated metabolic syndrome, non-alcoholic fatty liver disease, and cardiovascular diseases, as well as an increased risk of malignant tumors.[5–7]

The correlation between high-sugar diets and cancer cell progression is typically explained by metabolic changes, such as obesity or high insulin levels in DM patients or tumor cell proliferation at high-glucose concentration for *in vitro* experiments.[8–12] Cancer cell progression is explained as the result of pathological changes associated with weight gain and changes in energy metabolism from a long-term high-sugar diet.[13,14] These explanations create the misconception that all sugar should be avoided in many cancer patients, leading to unnecessary anxiety. Sugar, primarily glucose, is a source of energy for all cells, including immune cells.[15] When sugar levels are low, the body produces glucose from other sources, suggesting that under normal physiological and metabolic conditions there is no need to avoid sugar.[16] A sudden and drastic reduction in sugar intake may induce stress, raising blood sugar levels by increasing stress hormones and lowering immune function.[17,18] Thus, further studies should be conducted to evaluate whether eliminating sugar from the diets of cancer patients is advantageous.

In a mouse model of colorectal cancer, a short-term high-sugar diet adversely affects cancer formation and progression.[19] Oral administration of high fructose corn syrup in adenomatous polyposis coli mutant mice increases the glucose and fructose concentration in the intestinal lumen, resulting in the activation of glycolysis and the synthesis of fatty acids in tumor cells and tumorigenesis in the colonic epithelium.[19] Thus, in a colorectal cancer model, a high-sugar diet demonstrated a pro-tumor effect without inducing metabolic changes such as diabetes in the host.[20,21] Despite studies on the role of sugar in a colorectal cancer model, in which the colon is directly affected by glucose, little is known about the role of a high-sugar diet on other cancers, such as glioblastoma (GBM).

GBM, the most malignant brain tumor, seems to be unrelated to the gut; however, there is a close connection between the gut and the brain via the gut-brain axis.[22–24] In addition to the direct interaction via the vagus nerve and several hormones, various

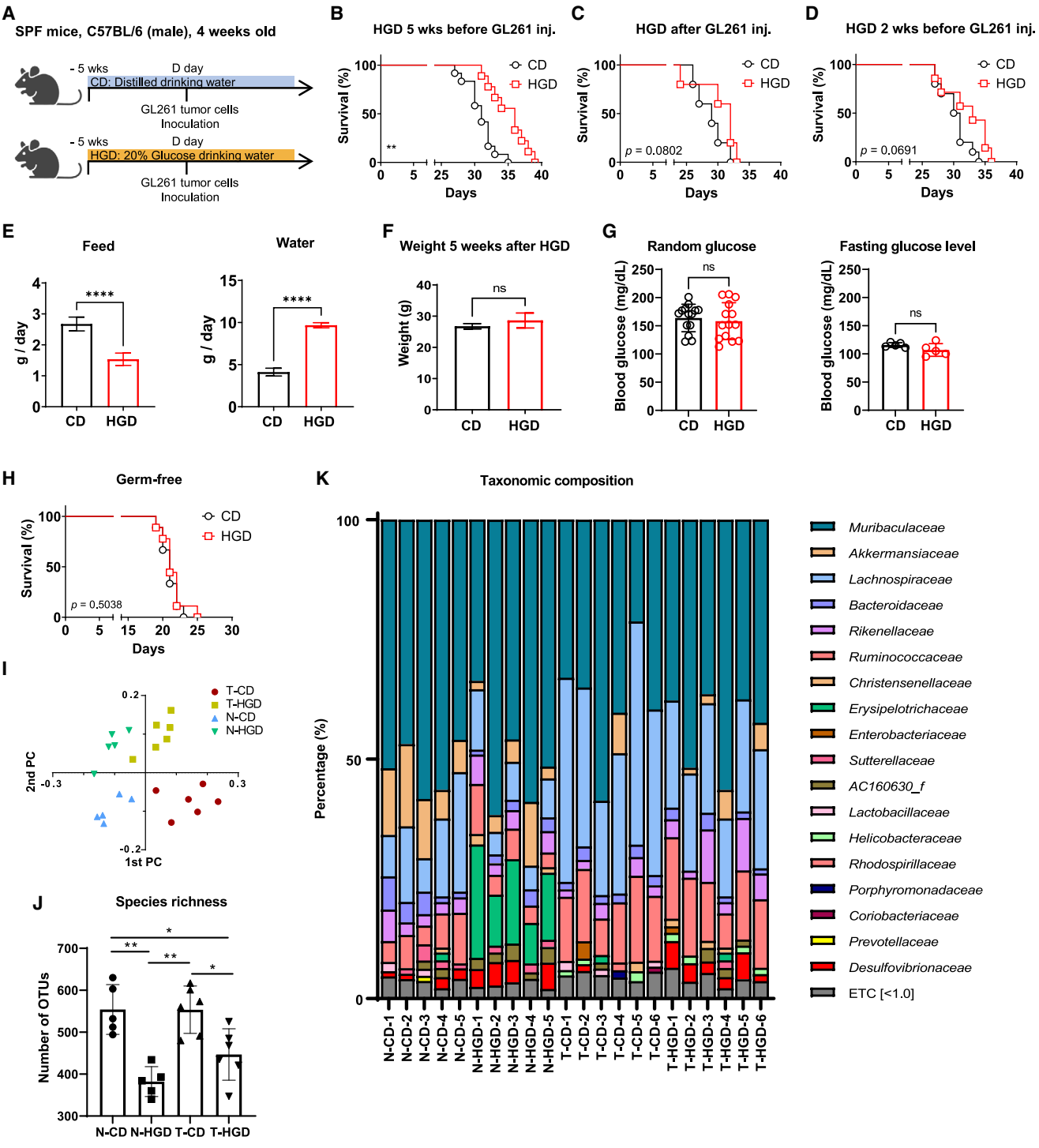

Figure 1. Supplementation with a high-glucose drink improved the survival rate in a glioblastoma mouse model through the gut microbiota

(A) Schema for experiments using SPF mice inoculated with GL261 mouse glioma tumor cells and fed a high-glucose drink (HGD) or a control drink (CD).

(B) Median survival of CD (31 days; n = 12) was compared with that of HGD (36 days; n = 11, p = 0.0024) by log-rank analysis for 5 weeks prior to inoculation with GL261 mouse glioma tumor cells.

(C) Median survival of CD (29 days; n = 5) was compared with that of HGD (32 days; n = 5, p = 0.0802) by log-rank analysis just after inoculation with GL261 mouse glioma tumor cells.

(D) Median survival of CD (30.5 days; n = 10) was compared with that of HGD (33 days; n = 7, p = 0.0691) by log-rank analysis for 2 weeks prior to inoculation with GL261 mouse glioma tumor cells.

(legend continued on next page)

metabolites produced by the gut microbiota also directly affect the brain.[22,25,26] Therefore, diets that affect the gut microbiota are gaining attention.[27,28] For example, in various tumor models, the gut microbiota enhances the efficacy of immune checkpoint inhibitors (ICIs) such as anti-PD-1.[29–33] Although diets that modulate the gut microbiota may also affect the anti-tumor immune response, there are no studies of whether changes to the gut microbiota enhance the anti-tumor immune response in GBM.

Here, we determined the effects of short-term supplementation with a high-glucose drink (HGD) on GBM growth and the anti-tumor immune response in mice. We performed experiments within the context of a high-sugar diet, specifically considering diet scenarios in which high levels of glucose were included in the drinking water, and found that short-term HGD supplementation increased the survival rate of GBM mice without inducing metabolic disease. In addition, we found that changes to the gut microbiota were associated with an improvement in GBM survival and induced an increase in the anti-tumor immune response to GBM through both quantitative and qualitative increases of cytotoxic $CD4^+$ T cells.

RESULTS

Increased survival of GL261 syngeneic tumor model mice receiving HGD supplementation via gut microbiota modulation

To determine the role of HGD supplementation in the GBM mouse model, we determined survival with or without HGD supplementation (Figure 1A). We induced an orthotopic syngeneic murine brain tumor model by injecting mice with GL261 GBM cells and provided an HGD by supplementing the drinking water with 20% dextrose. There was no improvement in the survival rate of mice on an HGD compared to the normal water control drink (CD) if the HGD was administered after GL261 tumor cell inoculation or for 2 weeks before GL261 tumor cell inoculation (Figures 1C and 1D). However, HGD supplementation for 5 weeks before GL261 tumor cell inoculation resulted in a significant improvement in GBM mouse survival (Figure 1B). Additionally, we found that HGD supplementation induced significantly better survival outcomes when using a different mouse GBM tumor cell line, CT-2A, under the same conditions (Figure S1A). We observed a 2-fold increase in water intake for the HGD group compared to the CD group, with a compensatory 50% reduction in food intake for the HGD group (Figure 1E) and no significant difference in the mean body weight between the CD and HGD groups (Figure 1F). We also measured glucose concentrations in blood from the tail vein and found no significant differences in random and fasting glucose level between the CD and HGD groups (Figure 1G). Therefore, a 5-week HGD did not induce DM or weight gain. To determine whether a change in weight alone affected survival, we compared the survival rate of GBM mice fed a high-fat diet (HFD) to induce weight gain (Figure S1B). Although the HFD mice gained weight, there was no significant difference in survival compared to the control group (Figure S1C).

In contrast, when the HGD experiment was performed in germ-free (GF) mice lacking gut microbiota, there was no difference in survival between the CD and HGD groups (Figure 1H). Therefore, we concluded that HGD supplementation improved the survival of GBM mice through the gut microbiota. Next, we performed 16S ribosomal RNA sequencing (RNA-seq) on fecal samples from each mouse to investigate the effect of HGD supplementation for 0, 2, and 5 weeks on the composition of the gut microbiota. The group that consumed the HGD for 5 weeks showed a significant change in species richness compared to the other groups that consumed the HGD for 0 and 2 weeks (Figure S1D). In principal coordinates analysis (PCoA) and unweighted pair group method with arithmetic mean clustering analysis, the group fed the HGD for 5 weeks formed a more distinct cluster that was separated from the others (Figures S1E and S1F). The relative ratios of the bacterial families in the consortia demonstrated differentiation at 5 weeks compared to 0 and 2 weeks (Figure S1G). These results suggest that significant changes in gut microbiota composition due to HGD supplementation required at least 5 weeks of HGD consumption. We then characterized the changes induced by HGD supplementation to the gut microbiota in the GBM mouse model by sequencing 16S ribosomal RNA genes from the feces of four mouse groups based on the presence or absence of tumors or HGD supplementation. Based on the PCoA plot, the gut microbiota for each of the four groups of mice was representative of their group and was affected by not only the HGD but also the presence or absence of brain tumors (Figure 1I). Mice without tumors given the HGD showed a significant decrease in operational taxonomic units, and even when tumors were present HGD supplementation induced the same effect on the gut microbiota (Figure 1J). The relative ratios of the bacterial families in the consortia for each group were affected markedly by HGD supplementation and GBM (Figure 1K). Thus, our data showed that relatively long-term HGD supplementation affected the gut microbiota independent of the presence of brain tumors.

(E) Mean daily food (left) and water (right) consumption per mouse on an HGD or CD.
(F) Mean weight of mice at the time of GL261 tumor cell inoculation for each group.
(G) Tail vein blood glucose levels for mice in the CD and HGD groups; random glucose level (left) and 4-h-fasting glucose level (right).
(H) Median survival of CD (21 days; n = 9) was compared with that of HGD (21 days; n = 9, p = 0.5038) by log-rank analysis for 5 weeks prior to inoculation with GL261 mouse glioma tumor cells in germ-free (GF) mice.
(I) Principal component (PC) analysis plot of the gut microbiota for each group. N-CD, normal brain and control drink; N-HGD, normal brain and high-glucose drink; T-CD, tumor brain and control drink; T-HGD, tumor brain and high-glucose drink.
(J) Alpha diversity of gut microbiota species richness by operational taxonomic units for each group.
(K) Taxonomic composition of the gut microbiota at the family level based on 16S rRNA gene sequencing of mouse feces for each mouse.
Data represent the mean ± standard error of the mean. Survival comparison results represent two or more independent experiments. ns, not significant; $^*p < 0.05$, $^{**}p < 0.01$, $^{***}p < 0.001$, $^{****}p < 0.0001$.

Single-cell RNA sequencing revealed that HGD supplementation enhanced the anti-tumor immune response in GBM mouse model

To determine whether the increased survival of GBM mice fed an HGD was due to an anti-tumor immune response, we repeated the experiment described above using NOD/Shi-scid, IL-2Rγnull (NOG) immunodeficient mice (Figure 2A). Similar to wild-type (WT) mice, the NOG mice did not show a significant increase in body weight with HGD supplementation (Figure 2B). However, unlike WT mice, there was no increase in the survival rate by HGD supplementation in NOG mice (Figure 2C). Therefore, the increase in the survival rate by HGD supplementation in WT mice was achieved through the regulation of the anti-tumor immune response.

To determine the changes in immune cells caused by HGD supplementation in the GBM tumor microenvironment (TME), we performed single-cell RNA-seq (scRNA-seq) analysis on CD45.2$^+$ tumor-infiltrating immune cells from mouse brains collected 20 days after GL261 tumor cell inoculation for the CD and HGD groups (Figure 2D). We found mostly myeloid cells, such as monocytes, macrophages, dendritic cells, and microglia, with lower proportions of T cells, natural killer (NK) cells, and B cells (Figure 2E). Although there was no significant difference in the proportions of immune cells, the frequency of T cells increased slightly in the HGD group, and the percentage of monocytes and macrophages tended to decrease (Figure 2F). To identify changes in gene expression, we analyzed differentially expressed genes (DEGs) in all immune cells, and volcano plots showed that the greatest change in gene expression in CD vs. HGD cells was in T cells (Figures 2G and S2A–S2F). A subcluster analysis of T cells showed that the frequency of CD8$^+$ cytotoxic T cells increased slightly, and the frequency of Foxp3$^+$ regulatory T cells (Tregs) decreased in the HGD group (Figure 2H). In the HGD group, the increase in the CD8$^+$ T cell/Foxp3$^+$ Treg ratio was much greater than the increase in the CD4$^+$ T cell/Foxp3$^+$ Treg ratio (Figure 2I). The ratios of CD4$^+$ and CD8$^+$ T cells to CD4$^+$ FOXP3$^+$ Tregs were measured at the protein level by fluorescence-activated cell sorting (FACS). There were no significant differences in numbers of CD4$^+$ and CD8$^+$ T cells between the CD and HGD groups (Figures S3A and S3B). However, the CD4$^+$ T cell/FOXP3$^+$ Treg ratio and CD8$^+$ T cell/FOXP3$^+$ Treg ratio were increased in the HGD group (Figure 2J).

To investigate whether HGD had an impact on not only immune cells but also tumor cells within the TME, we performed scRNA-seq on tumor cells. Tumor cells were found to be organized into two main clusters, with cluster 0 present at a slightly higher frequency in the CD group compared to the HGD group (Figure S4A). This cluster showed elevated expression of hypoxia-inducible factor 1 subunit α and solute carrier 2 family member 1, which encodes glucose transporter 1 (Figure S4B). Additionally, gene set enrichment analysis (GSEA) revealed higher expression of the hypoxia-related gene set, indicating that tumor cells in the CD group had greater hypoxic status compared to tumor cells in the HGD group (Figure S4C). However, there was no significant difference in the expression levels of the gene sets related to tumor cell proliferation between the two groups. In particular, no differences were observed in metabolic-related gene sets such as those involved in glycolysis or fatty acid metabolism, suggesting that oral administration of glucose did not have a direct effect on the tumor (Figure S4D). Thus, the survival gain by HGD supplementation seems to occur through inducing changes in the ratio of cytotoxic CD8$^+$ T cells and helper CD4$^+$ T cells to regulatory T cells, rather than having a direct effect on tumor cells.

Probiotics did not increase anti-PD-1 efficacy in the GBM mouse model

In human and mouse models, GBM is highly immunosuppressive and largely unresponsive to anti-PD-1 ICIs. We also found no effect of anti-PD-1 ICIs in our GL261 mouse orthotopic tumor model (Figure S5B). Because the gut microbiota influenced the anti-tumor immune response of GBM, we determined whether the efficacy of anti-PD-1 ICIs in GBM could be enhanced by oral administration of commercially available probiotics that can induce changes in the gut microbiota (Figure S5A). However, none of the probiotics had a significant effect on the survival rate via synergistic action with anti-PD-1 ICIs (Figures S5C–S5F). Thus, it appears that common probiotic strains had no significant role in regulating anti-tumor immune responses in the GBM mouse model.

Interferon-related genes in CD8$^+$ T cells in the GBM tumor microenvironment from mice supplemented with HGD had a critical role in the anti-tumor immune response

To measure the differences in DEGs in CD8$^+$ T cells from the CD vs. HGD groups, we analyzed T cell subclusters using previous scRNA-seq data. Subclusters of T cells in the scRNA-seq data identified two clusters of CD8$^+$ T cells, with a dramatic increase in cluster 0 in the HGD group (Figure 3A). GSEA of the CD8$^+$ T cell subcluster revealed increased interferon-γ (IFN-γ) and IFN-α responses in cluster 0 (Figure 3B). In this subcluster, expression of interferon-stimulated genes (ISGs) *Isg15*, *Ifi27l2a*, *Ifit1*, *Ifit2*, and *Ifit3* increased, and expression of *Isg20*, *Ifitm1*, *Ifitm2*, and *Ifitm3* decreased (Figure 3C). Based on The Cancer Genome Atlas (TCGA) data, high expression of *Isg15*, *Ifit1*, *Ifit2*, *Ifit3*, and *Ifi27l2a* genes was associated with an increased survival rate, whereas expression of the *Ifitm1*, *Ifitm2*, and *Ifitm3* genes was not significantly associated with the survival rate in GBM patients (Figure 3D). Thus, the provision of the HGD was related to not only the frequency of CD8$^+$ T cells but also the expression levels of some ISGs that were associated with better survival in humans.

To confirm that these changes in CD8$^+$ T cells induced by HGD supplementation improved the survival rate, we used a CD8 depletion antibody to determine the effect of HGD supplementation on GBM survival in a CD8$^+$ T cell-depleted mouse model. There was no increase in the survival rate with HGD supplementation in the CD8$^+$ T cell-depleted mouse model (Figure 3E). The anti-PD-1 effect was absent in the CD group but present in the HGD group (Figures 3F and 3G). Taken together, the data confirmed that HGD supplementation enhanced the anti-tumor immune response through changes in cytotoxic CD8$^+$ T cells and that the anti-PD-1 effect was induced by HGD supplementation in a GBM mouse model.

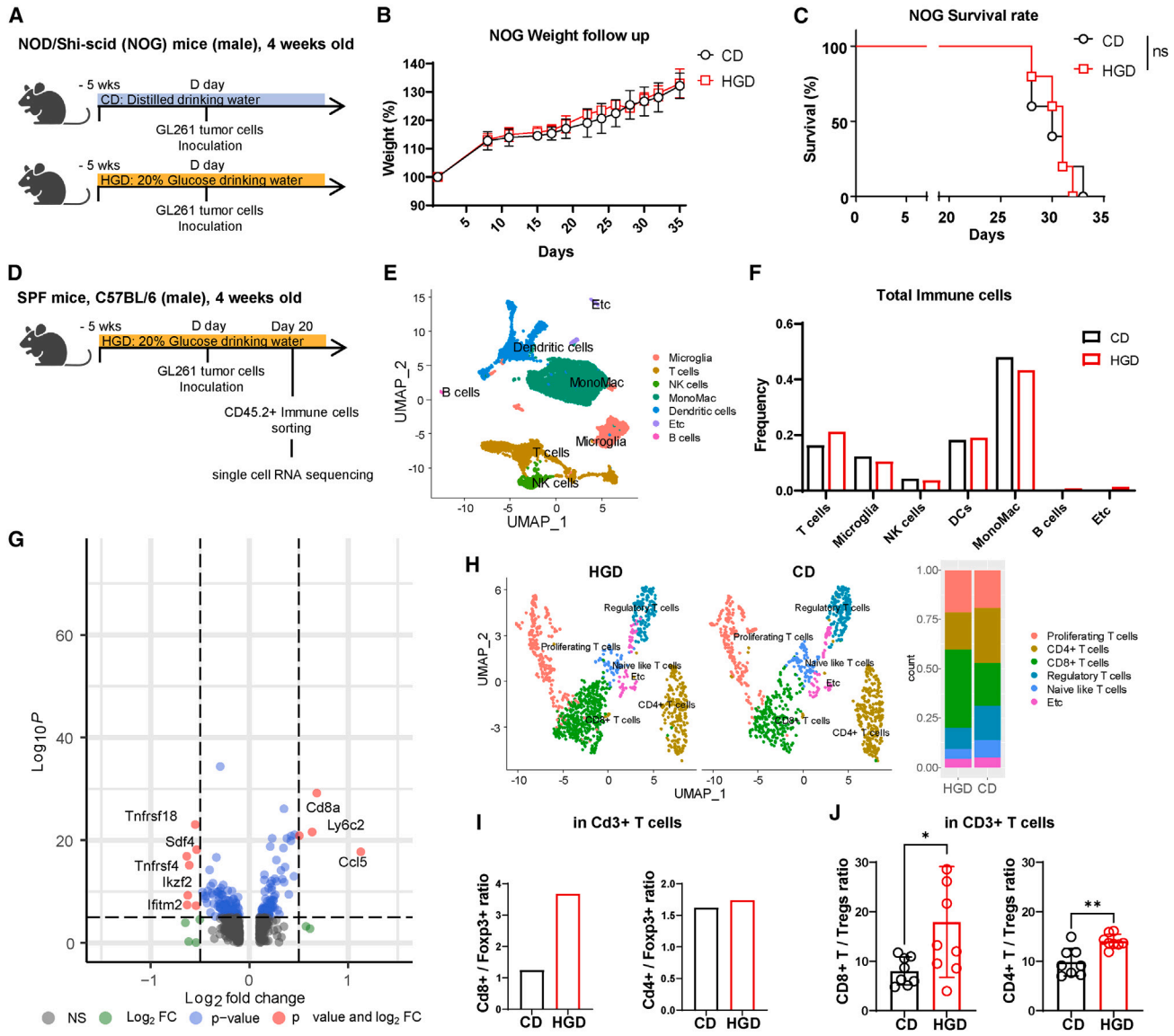

Figure 2. HGD supplementation enhanced the CD8$^+$ T cell-mediated anti-tumor immune response in a glioblastoma mouse model

(A) Schema for experiments using NOD/Shi-scid, IL-2Rγnull (NOG) immunodeficient mice inoculated with GL261 mouse glioma tumor cells and fed an HGD or CD.

(B) Mean weight of NOG mice on a 5-week HGD or CD measured prior to GL261 tumor cell inoculation.

(C) Median survival of CD (30 days; n = 5) was compared with that of HGD (31 days; n = 5, p = 0.9640) by log-rank analysis for 5 weeks prior to inoculation with GL261 mouse glioma tumor cells in NOG mice.

(D) Schema for experiments for single-cell RNA sequencing (scRNA-seq) analysis of mouse CD45.2$^+$ immune cells in the GBM tumor microenvironment (TME).

(E) Uniform manifold approximation and projection (UMAP) plot showing immune cells clustered by their gene expression profiles. NK cells, natural killer cells; MonoMac, monocytes and macrophages.

(F) Comparison of immune cell frequencies in the mouse GBM TME for the CD and HGD groups.

(G) Volcano plot of T cells. Each dot represents one gene, and the $\log_2$ fold change indicates the mean expression level of each gene. Red dots represent genes that were significantly differentially expressed between the CD and HGD groups. Dots on the right side indicate genes upregulated in the HGD group, and dots on the left side indicate genes upregulated in the CD group.

(H) UMAP of T cell subclusters (left), and a bar plot showing the frequency of each T cell subcluster (right) between HGD and CD groups.

(I and J) Bar graphs comparing the ratios of CD8$^+$ T cells to Foxp3$^+$ regulatory T cells (Tregs) (left) and CD4$^+$ T cells to Foxp3$^+$ Tregs (right) between CD and HGD groups based on scRNA-seq data (I) and fluorescence-activated cell sorting (FACS) analysis (J).

Changes in survival rate and FACS data were determined using two or more independent experiments. ns, not significant; *p < 0.05, **p < 0.01.

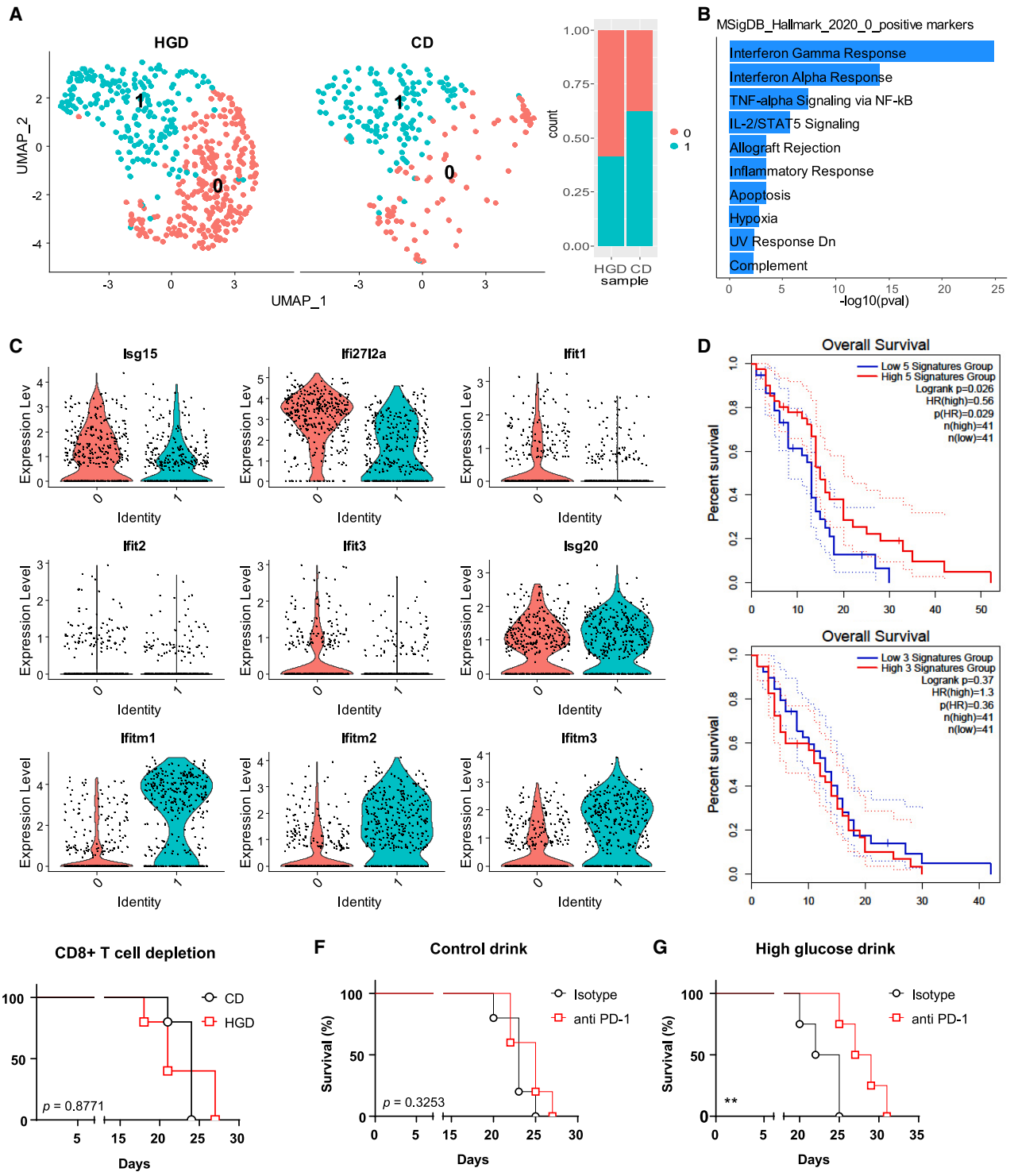

Figure 3. Phenotypic changes in CD8$^+$ T cells in the GBM TME in the CD vs. HGD groups

(A) UMAP analysis of subclusters of CD8$^+$ T cells (left), and a bar plot of the frequency of each cluster (right) for HGD vs. CD groups.

(B) Functional enrichment analysis with differentially expressed genes of cluster 0 compared to cluster 1 using enrichR and the Hallmark 2020 database.

(C) Violin plot comparing *Isg15*, *Ifi27l2a*, *Ifit1*, *Ifit2*, *Ifit3*, *Isg20*, *Ifitm1*, *Ifitm2*, and *Ifitm3* expression in CD8$^+$ T cells in the CD vs. HGD groups.

(D) Survival analysis using the TCGA GBM dataset showing that the interferon-stimulated gene set, which was highly expressed in the HGD group (*Isg15*, *Ifi27l2a*, *Ifit1*, *Ifit2*, and *Ifit3*), correlated with improved patient survival (top), whereas a gene set that showed low expression in the HGD group (*Ifitm1*, *Ifitm2*, and *Ifitm3*) did not correlate with improved survival in patients in the TCGA database (bottom).

(legend continued on next page)

An HGD-induced increase in the Desulfovibrionaceae family in the gut microbiota inhibited GBM tumor growth

We determined that the gut microbiota was affected by HGD supplementation through 16S rRNA gene sequence analysis; however, the presence or absence of tumors also affected the microbiota (Figure S6A). When the bacterial strains showing significant changes following HGD supplementation were placed into groups based on the presence or absence of tumors and ranked according to the linear discriminant analysis effect size, there were strains with similar changes in each group (Figures S6B and S6C). Family-level bacteria that increased significantly in the guts of mice with a normal brain on HGD supplementation included Erysipelotrichaceae, Desulfovibrionaceae, and *AC160630*_f strains, whereas *FR888536*_f and Prevotellaceae strains decreased (Figure 4A). In the guts of mice with GL261 tumors, Rikenellaceae, Desulfovibrionaceae, and Odoribacteraceae strains increased with HGD supplementation, whereas *FR888536*_f, Phophyromonadaceae, Lactobacillaceae, and Lachnospiraceae strains decreased (Figure 4B). Among these, only the strains of the Desulfovibrionaceae family increased in the guts of mice on HGD supplementation, regardless of the presence or absence of tumors (Figure 4C). When examining the changes in the Desulfovibrionaceae ratio over the course of HGD supplementation, it was found that provision of the HGD for 2 weeks did not induce a significant increase in this strain (Figure S7A). However, provision of an HGD for 5 weeks induced a significant increase in the Desulfovibrionaceae ratio (Figure S7A). Therefore, we hypothesized that the HGD might impact the gut colonization of Desulfovibrionaceae. Thus, following oral gavage of Desulfovibrionaceae, we assessed the gut colonization capability of Desulfovibrionaceae in response to HGD supplementation. One week after discontinuing the oral gavage of Desulfovibrionaceae, DNA abundance of Desulfovibrionaceae strain in mouse feces revealed that when the strain was administered without HGD supplementation, there was no significant increase in strain abundance compared to the control group. However, in cases in which the HGD was supplied, a significant increase in the Desulfovibrionaceae strain ratio was observed. Notably, the highest abundance was observed when both the administration of *Desulfovibrio vulgaris* and HGD supplementation were carried out simultaneously (Figure S7B). These results suggest that HGD supplementation has a positive impact on the gut colonization of Desulfovibrionaceae strains.

To determine whether the presence of strains in the Desulfovibrionaceae family enhanced the anti-tumor immune response of the HGD group in GBM mice, we administered *Desulfovibrio vulgaris*, which is present in the normal gut microbial environment, to antibiotic-cocktail-treated mice depleted of gut microbiota (Figure 4D). The control HGD group showed no increase in survival rate (Figure 4E), but in the group treated with *D. vulgaris* by oral gavage, the HGD group showed a significant increase in the survival rate of the GBM mouse model (Figure 4F). Furthermore, we investigated the impact of the oral administration of *Faecalibaculum rodentium* and *Alistipes shahii* strains, which were shown to be increased following HGD supplementation, on the survival rate of the GBM mouse model under HGD supplement in antibiotics-treated mice. We found that there was no significant increase in the survival rate of these strains (Figures S8A and S8B). These results suggested that the increased Desulfovibrionaceae strain abundance following HGD supplementation may be a contributing factor to their increased survival rate of the GBM mouse model.

To compare tumor growth between CD and HGD mice that were administered *D. vulgaris* by oral gavage, we inoculated mice with GL261-green fluorescent protein (GL261-GFP) cell lines under the same conditions, and the brains were collected 20 days later to compare the frequency and number of $CD45.2^{-}GFP^{+}$ tumor cells. The GFP^{+} tumor cell frequency was significantly lower in the HGD group than in the CD group for those that received *D. vulgaris*, and the number of $CD45.2^{-}GFP^{+}$ tumor cells was also decreased in the HGD group (Figures 4G and 4H). In addition, confocal images of brains removed 21 days after mice were inoculated with GL261-GFP showed central necrosis in almost all CD mice (Figures 4I and 4J) but minimal central necrosis in the HGD group (Figures 4I and 4J). Because central necrosis is an indicator of rapid tumor growth,[34] this difference suggested that HGD supplementation was important in inhibiting tumor growth for *D. vulgaris*-treated mice. Therefore, we conclude that HGD supplementation inhibited GBM tumor progression and that Desulfovibrionaceae strains in the gut microbiota played a key role in the anti-tumor immune response of HGD supplementation.

Desulfovibrionaceae induced by HGD supplementation influences the anti-tumor immune response in GBM in a metabolically activated state

To identify how Desulfovibrionaceae induced by HGD supplementation regulates the anti-tumor immune response in brain tumors, we first aimed to understand its impact on the gut immune system by examining changes in the mesenteric lymph nodes (mLNs). Because mLNs are closely associated with the gut immune system,[35] we hypothesized that if HGD supplementation had an impact on the gut immune system, changes might occur in the immune cell populations within the mLNs. However, no significant differences were observed in the total frequencies of $CD8^{+}$ and $CD4^{+}$ T cell subtypes between the CD and HGD groups (Figures S9A and S9B). These results suggest that HGD consumption alone did not induce significant changes in the gut immune system. Previous reports have indicated that glucose can impair gut barrier integrity.[36] Therefore, we investigated the effect of HGD supplementation on gut barrier integrity by orally administering 4-kDa fluorescein isothiocyanate-conjugated dextran to

(E) Median survival of CD (24 days; n = 5) was compared with that of HGD (21 days; n = 5, p = 0.8771) by log-rank analysis in $CD8^{+}$ T cell-depleted GBM model mice, generated using an anti-mouse CD8 depletion antibody.
(F and G) Median survival of mice treated with isotype (23 days; n = 5) by log-rank analysis was compared with that of anti-PD-1 (25 days; n = 5, p = 0.3253) with CD (F), and median survival of isotype (23.5 days; n = 4) was compared with that of anti-PD-1 (28 days; n = 4, p = 0.0285) with HGD (G) for 5 weeks prior to inoculation with GL261 mouse glioma tumor cells.
Survival comparison results represent three independent experiments. *p < 0.05, **p < 0.01.

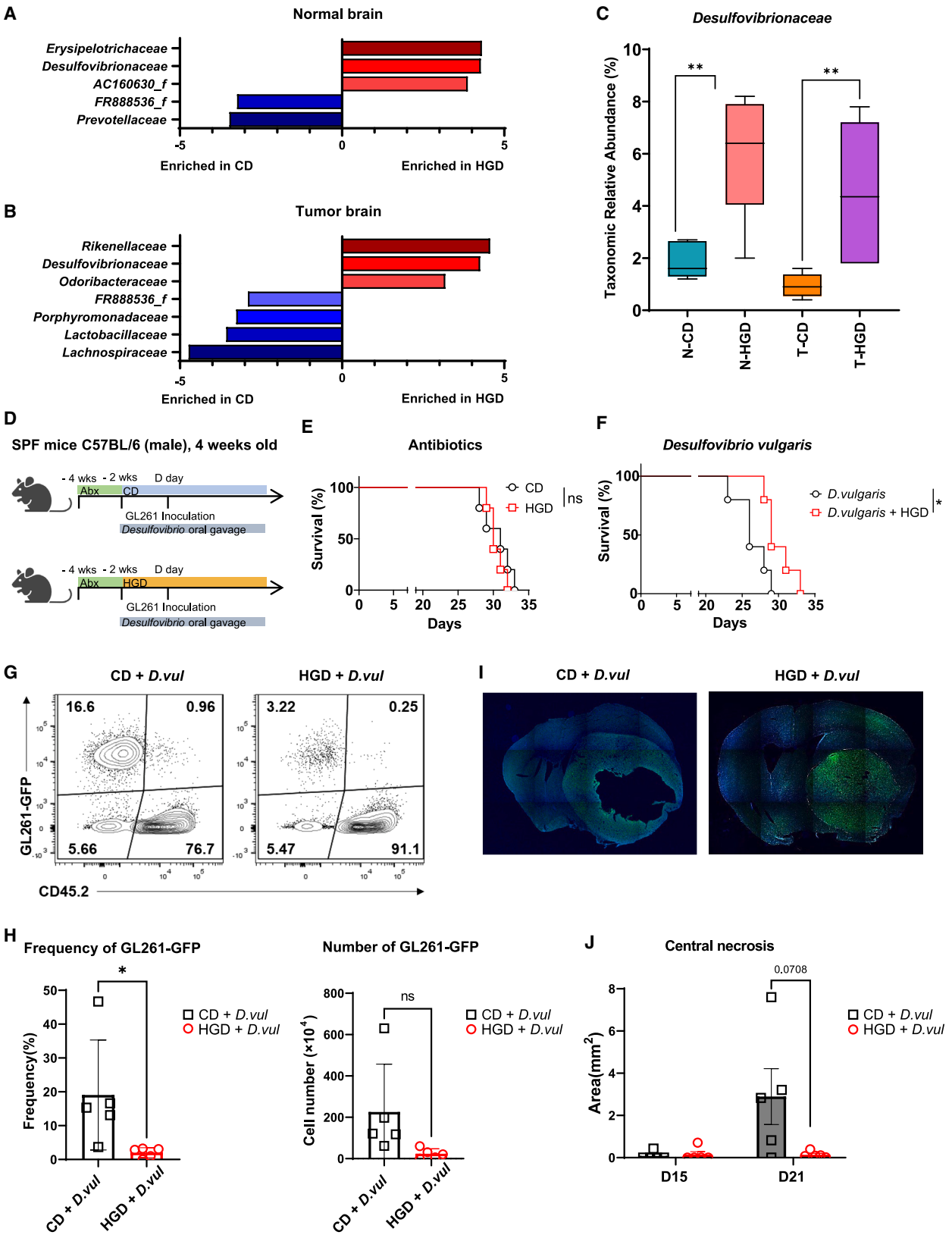

(legend on next page)

mice and then measuring its concentration in the bloodstream. The results revealed a significant increase in the bloodstream concentration of dextran in mice subjected to HGD supplementation, indicating increased gut permeability, particularly in GF mice (Figure S9C). However, in specific pathogen-free (SPF) mice, although HGD supplementation led to increased gut permeability, the significance of the difference was borderline, suggesting a reduced effect (Figure S9D). Considering that these changes in permeability might lead to the increased penetration of pathogen-associated molecular patterns rather than the metabolic byproducts of Desulfovibrionaceae, the survival rate of the mouse lines were compared following the administration of heat-inactivated Desulfovibrionaceae under the same experimental conditions. However, administration of the inactivated strain did not result in a significant increase in survival rate (Figure S9E). Based on these experimental results, it can be speculated that the metabolic activation of this strain likely played a crucial role in the increased survival rate of the GBM mouse model.

Oral gavage of *Desulfovibrio* bacteria in GF mice induced gene expression changes for CD8$^+$ T cells, similar to SPF mice fed an HGD

To determine whether *Desulfovibrio* regulates the anti-tumor immune response associated with HGD supplementation, we performed oral gavage with a *Desulfovibrio* strain vs. a Dulbecco's phosphate-buffered saline (DPBS) control in a GF GL261 mouse tumor model with HGD supplementation (Figure 5A). Brains were collected 20 days after GL261 tumor inoculation, and scRNA-seq analysis of isolated CD45.2$^+$ immune cells (Figure 5A) showed an increased frequency of cytotoxic CD8$^+$ T cells (Figure 5B) and increased expression of ISGs in the group that received oral gavage with *Desulfovibrio* (Figure 5C). These changes were similar to those seen in cytotoxic CD8$^+$ T cells in the scRNA-seq data for SPF mice on an HGD. A violin plot of representative T cell clusters showed these changes only in CD8$^+$ T cells (Figure 5D). In addition, we found low expression levels of genes encoding the PD-1, cytotoxic T lymphocyte-associated protein 4, T cell immunoreceptor with immunoglobulin (Ig) and immunoreceptor tyrosine-based inhibitory motif domains, and T cell Ig and mucin-containing protein-3 exhaustion marker proteins in CD8$^+$ T cells with high expression of ISGs in the scRNA-seq data for SPF mice (Figure 5E). We also checked the expression levels of activation marker proteins coding genes such as *Cd69* and *Il2ra*, but there was no spatial correlation with high ISG expression (Figures S10A and S10B). Moreover, we found that treatment with *D. vulgaris* not only enhanced anti-PD-1 in mice on an HGD that received a GL261 tumor inoculation but also delayed weight loss after inoculation (Figure 5F) and increased the survival time (Figure 5G). We also observed a synergistic effect of HGD supplementation + *D. vulgaris* oral gavage in mice that were treated with anti-PD-1 ICIs (Figure 5G). Based on these results, we demonstrated that the *D. vulgaris* played a significant role in T cell-mediated anti-tumor immune response and acted as a key mediator in facilitating the synergistic effect with anti-PD-1.

NKG2D$^+$ cytotoxic CD4$^+$ T cells in the glioblastoma TME

A subcluster analysis of CD4$^+$ T cells based on scRNA-seq data identified three clusters (Figure S11A) with high *Cd4* mRNA expression (Figure S11B). Subclusters of clusters 0 and 2 expressed cytokine- and chemokine-encoding genes such as *Ifng*, *Ccl1*, *Ccl2*, *Ccl3*, and *Tnfsf8* (Figure S11C). However, we found increased expression of *Klrk1*, encoding NKG2D, and *Klrd1* and *Gzmb*, encoding granzyme B, in cluster 1 (Figure S11C). The violin plot showed higher expression of *Klrk1*, *Gzmb*, and *Lamp1*, encoding CD107a, in cluster 1 than in the other clusters (Figure S11D). These genes are highly expressed in NK-like immune cells. GSEA showed that the score for gene sets related to NK-cell-mediated cytotoxicity was high in cluster 1 (Figure S11E). FACS analysis to distinguish cells based on proteins showed that CD107a$^+$CD4$^+$ T cells accounted for 30%–40% of the CD4$^+$ T cells in the GBM TME (Figure S11F). Although the frequency of CD107a$^+$ in CD4$^+$ T cells was lower than that in CD8$^+$ T cells, a significant number of cells showed NK-like features in CD4$^+$ T cells (Figures S11F and S11G). Additionally, NKG2D expression increased in CD107a$^+$IFN-γ^-CD4$^+$ T cells but not in CD107a$^+$IFN-γ^-CD8$^+$ T cells (Figure S11H). IFN-γ expression was lower, and granzyme B expression was higher, in NKG2D$^+$CD107a$^+$CD4$^+$ T cells than in conventional CD4$^+$ T cells (Figures S11I and S11J). In particular, granzyme B and NKG2D expression levels were lower in CD107a$^-$CD4$^+$ T cells than in cytotoxic CD8$^+$ T cells but higher in CD107a$^+$CD4$^+$ T cells than in cytotoxic CD107a$^+$CD8$^+$ T cells (Figures S11J and S11K). Taken together, our data indicate that

Figure 4. HGD supplementation inhibited GBM tumor growth when Desulfovibrionaceae family bacteria were present in the gut microbiota

(A and B) Linear discriminant analysis effect size analysis identified the most differentially abundant family-level taxa in the gut microbiota, comparing the CD and HGD groups in the absence (A) or presence (B) of brain tumors.

(C) Relative taxonomic abundance of the Desulfovibrionaceae family by group: N-CD, normal brain and control drink; N-HGD, normal brain and high-glucose drink; T-CD, tumor brain and control drink; T-HGD, tumor brain and high-glucose drink.

(D) Schema for experiments to determine the effect of *Desulfovibrio* (*D. vulgaris*) on the GL261 mouse GBM model.

(E and F) Median survival of CD (31 days; n = 5) by log-rank analysis was compared with that of HGD (33 days; n = 5, p = 0.5467) treated with antibiotics (E), and median survival of CD (26 days; n = 5) was compared with that of HGD (29 days; n = 5, p = 0.0299) with oral gavage of *D. vulgaris* after antibiotics treatment (F).

(G) Representative FACS plots for frequency analysis of GL261-GFP in the GBM TME cells for CD or HGD mouse groups treated with *D. vulgaris* after antibiotics treatment.

(H) Frequency and number of GFP$^+$ GL261 live tumor cells identified by Fixable Viability Stain 780 (FVS780) in the GBM TME cells for the CD and HGD mouse groups treated with *D. vulgaris* after antibiotics treatment.

(I) Representative confocal images of brains from CD (left) and HGD (right) mice treated with *D. vulgaris* shown in coronal sections. Blue, 4′,6-diamidino-2-phenylindole (DAPI); green, GFP.

(J) Central necrosis areas of mouse brain tumors on day 15 or day 20 in the CD and HGD mouse groups treated with *D. vulgaris*.

Survival results and FACS data represent two or more independent experiments. ns, not significant; *p < 0.05, **p < 0.01.

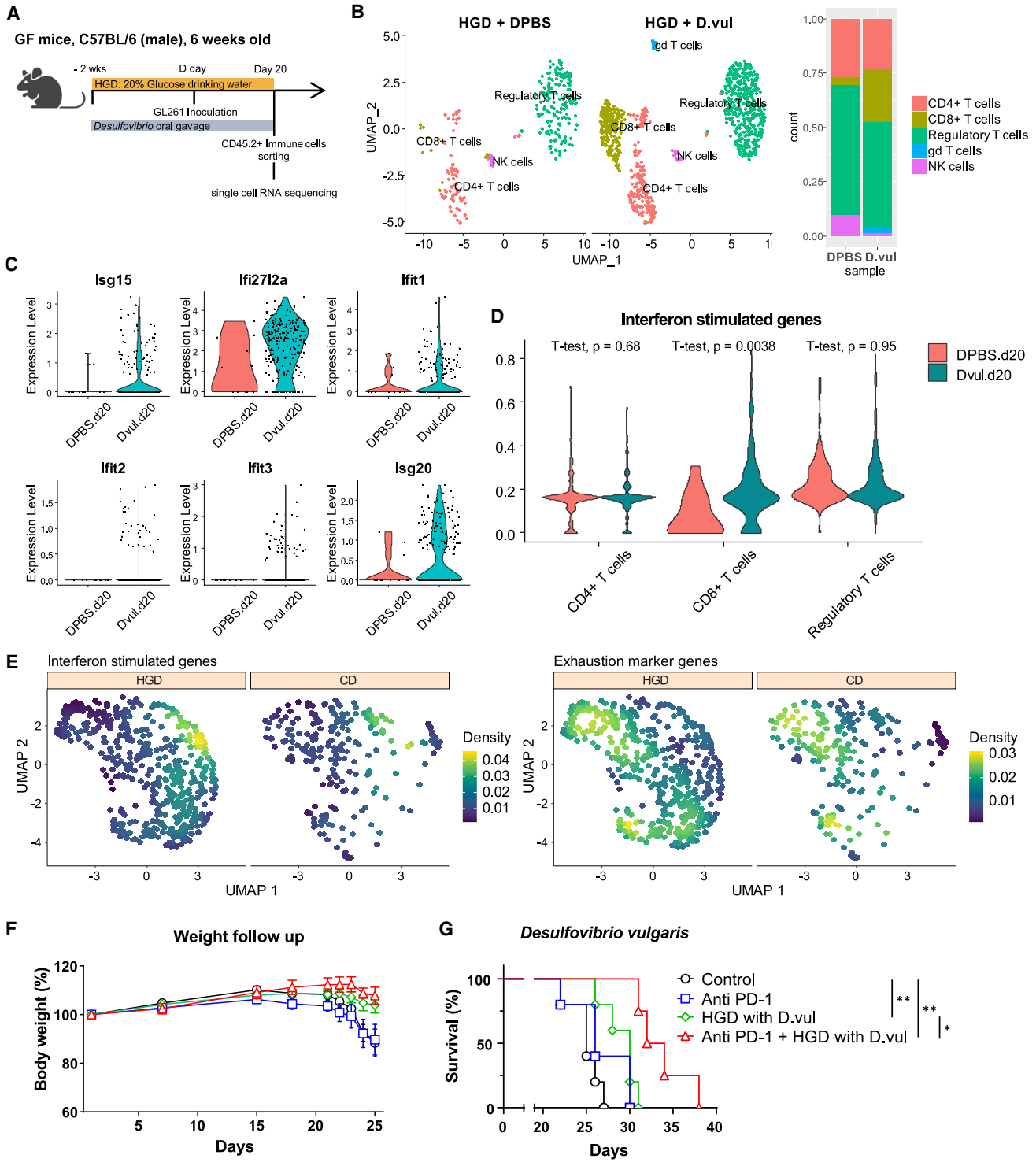

Figure 5. GF mice fed an HGD and supplemented with *D. vulgaris* had immune cells similar to those of SPF mice fed an HGD

(A) Schema for experiments using scRNA-seq to determine the effect of *D. vulgaris* on GL261 GBM model GF mice fed an HGD.

(B) UMAP plot of T cell subclusters in GF mice fed an HGD with or without *D. vulgaris* oral gavage (left), and a bar plot of the frequency of each cluster (right).

(C) Violin plot comparing the expression levels of *Isg15*, *Ifi27l2a*, *Ifit1*, *Ifit2*, *Ifit3*, and *Isg20* in CD8$^+$ T cells comparing DPBS.d20, oral gavage of Dulbecco's phosphate-buffered saline (DPBS), and Dvul.d20, oral gavage of *D. vulgaris* (D.vul).

(legend continued on next page)

$CD107a^+CD4^+$ T cells have expression levels of genes and proteins related to cytotoxicity similar to those usually expressed in cytotoxic $CD8^+$ T cells within the GBM TME.

Combination treatment with HGD supplementation and anti-PD-1 administration created more effective anti-tumor properties of T cells in glioblastoma

Through previous experiments, we determined that HGD supplementation has a synergistic effect with anti-PD-1 ICIs. To determine changes in immune cells in the TME in mice fed an HGD and treated with anti-PD-1 vs. the CD + anti-PD-1 control group, we performed scRNA-seq on $CD45.2^+$ immune cells (Figure 6A). We found no difference in the ratio of $CD8^+$ T cells to $Foxp3^+$ Tregs, but the ratio of $CD4^+$ T cells to $Foxp3^+$ Tregs increased in the HGD + anti-PD-1 group (Figure 6B). A violin plot showed that *Isg15*, *Ifi27l2a*, and *Isg20* expression increased in $CD8^+$ T cells (Figure 6C), and $CD4^+$ T cells also showed elevated expression of ISGs affecting the survival rate of HGD + anti-PD-1 vs. CD + anti-PD-1 cells (Figure 6D). Therefore, $CD8^+$ T cells and $CD4^+$ T cells in the HGD group were more affected by anti-PD-1 ICIs in the GBM mouse model.

A subcluster analysis revealed four clusters of $CD4^+$ T cells with a higher frequency for cluster 0 in the HGD + anti-PD-1 cells vs. CD + anti-PD-1 cells (Figure 6E). For gene sets related to cytotoxicity, a feature plot showed that expression of *Klrk1*, *Runx3*, *Gzmb*, *Ctla2a*, *Fasl*, *Klrd1*, and *Nkg7* was higher in cluster 0 than in other clusters (Figure 6F), indicating a higher frequency of cytotoxic $CD4^+$ T cells in the HGD + anti-PD-1 group. FACS analysis comparing cytotoxic $CD107a^+$ T cells in the CD + anti-PD-1 group with the HGD + anti-PD-1 group showed that the geometric mean fluorescence intensities of granzyme B and NKG2D in $CD107a^+$ cytotoxic $CD4^+$ T cells were similar with or without HGD supplementation (Figures 6G and 6H). However, the frequency of $CD107a^+$ cytotoxic $CD4^+$ T cells increased significantly with HGD supplementation (Figure 6I), although in mice depleted of $CD4^+$ T cells and treated with HGD + anti-PD-1, there was no significant increase in survival rate (Figure 6J). These results indicated that both $CD8^+$ T cells and $CD4^+$ T cells play an important role in the synergistic effect of HGD + anti-PD-1 on survival.

DISCUSSION

Our results show that HGD supplementation increased the survival rate of GBM mice and that the gut microbiota played a key role in linking the HGD with anti-tumor immunity. The relationship between gut microbiota and anti-tumor immunity is one of the most promising advances in cancer research.[37,38] However, research on the relationship between gut microbiota and anti-tumor immune response has mostly been conducted in immune-inflamed tumors, also called "hot tumors," such as melanoma, colon cancer, and lung cancer, which have highly active anti-tumor immune responses compared with other tumors.[39,40] The applicability of these gut microbiota studies to other types of tumors is not known. We demonstrated for the first time the importance of the gut microbiota to anti-tumor immune response in GBM, a non-inflamed tumor ("cold tumor"). We showed that the composition of the gut microbiota limited the number and function of cytotoxic T cells, which are generally considered to constitute a significant portion of the anti-tumor immune response. In addition, we showed that HGD supplementation acted on GBM by regulating T cell-mediated anti-tumor immune responses via gut microbiota modulation and that this effect was synergistic with anti-PD-1 ICIs.

Although we demonstrated that HGD supplementation benefited the anti-tumor immune response of GBM, the effects of HGD supplementation may not have similar effects on the whole host immune system. In fact, a reduction in dietary sugars could improve lifestyle-associated diseases and health.[41] Nevertheless, glucose is an important source of energy not only for cancer cells but also for normal cells, including immune cells.[16] There is insufficient evidence that a reduction in dietary glucose inhibits tumor growth, and more research is needed.[42] Hence, we have shown that a short-term HGD, which does not induce metabolic-associated diseases, enhanced the anti-tumor immune response of GBM through the gut microbiota. This suggests that other approaches and perspectives should be applied to studies of the effects of glucose on tumors.

It is well known that cytotoxic cells, including $CD8^+$ T cells, NK/T cells, NK cells, and $\gamma\delta$ T cells, are present in the GBM TME.[43] In contrast, $CD4^+$ T cells support the functions of these cytotoxic immune cells through cytokine secretion.[44,45] However, we found higher NKG2D and granzyme B expression levels in $CD107a^+NKG2D^+CD4^+$ T cells in the GBM TME than in cytotoxic $CD8^+$ T cells in the same GBM tissue. Although $CD107a^+NKG2D^+CD4^+$ T cells are not found in normal tissues, they are observed in autoimmune diseases, chronically inflamed tissues, and tumor tissues.[46] However, little is known about the function of this subset of cells or the environments in which they function.[47,48] We found greater changes in $CD107a^+NKG2D^+CD4^+$ T cells than in other immune cells in the GBM TME of mice on an HGD treated simultaneously with anti-PD-1. In addition, when CD4 was depleted by antibody treatment, no change in survival was observed, suggesting that $CD107a^+NKG2D^+CD4^+$ T cells played an important role in the positive effect of anti-PD-1 with HGD supplementation. These findings suggest a new target cell for the application of ICIs, which have shown little effect on GBM. Therefore, further research on cytotoxic $CD4^+$ T cells is needed.

(D) Expression levels of the interferon-stimulated genes set (*Isg15*, *Ifi27l2a*, *Ifit1*, *Ifit2*, *Ifit3*, and *Isg20*) in a violin plot of representative T cell subclusters, including $CD4^+$ T cell, $CD8^+$ T cell, and $Foxp3^+$ regulatory T cell clusters.

(E) Comparison of the combined expression levels of interferon-stimulated genes (left) and exhaustion marker genes (right) with a feature plot comparing the CD and HGD groups.

(F and G) Effects on weight (F) and survival (G) of a combination treatment for GBM model mice on an HGD by adding *D. vulgaris* (D.vul) and/or anti-PD-1 treatment for mice in four groups: Median survival of control (25 days, n = 5) vs. anti-PD-1 (26 days, n = 5, p = 0.1729), control vs. HGD with D.vul (30 days, n = 5, p = 0.0090), control vs. anti-PD-1 + HGD with D.vul (33 days, n = 4, p = 0.0046), and HGD with D.vul vs. anti-PD-1 + HGD with D.vul (p = 0.0120) by log-rank analysis. Survival comparison results represent two or more independent experiments. *p < 0.05, **p < 0.01.

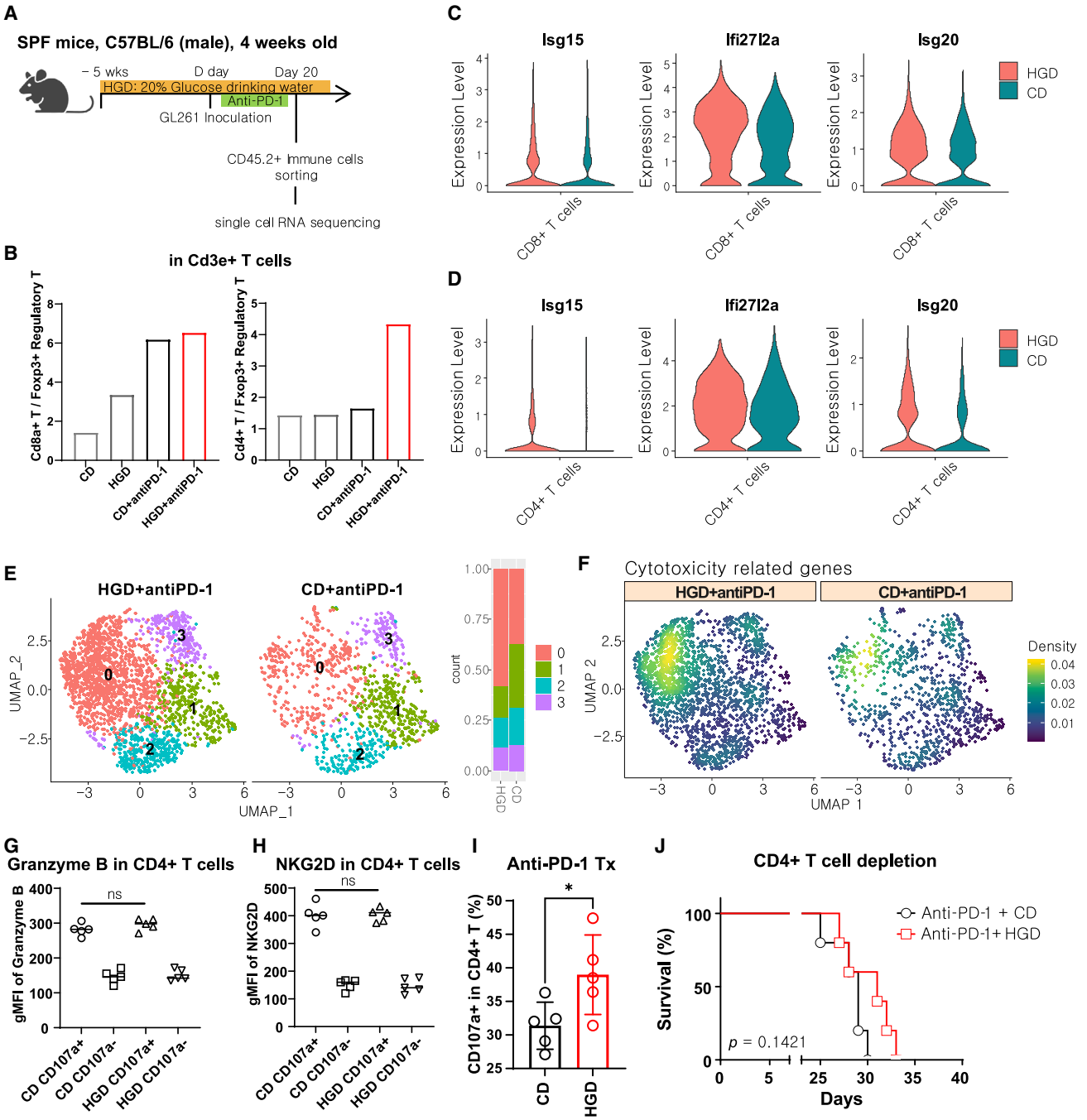

Figure 6. Combination treatment with HGD supplementation and anti-PD-1 administration increased the anti-tumor properties of T cells in GBM model mice

(A) Schema for experiments using scRNA-seq to determine the phenotypes of tumor-infiltrating T cells from the CD vs. HGD mouse groups administered an anti-PD-1 treatment.

(B) Comparison of the CD8$^+$ T cell/Foxp3$^+$ Treg and CD4$^+$ T cell/Foxp3$^+$ Treg ratios for the CD, HGD, CD + anti-PD-1, and HGD + anti-PD-1 groups.

(C and D) Violin plot comparing the expression levels of *Isg15*, *Ifi27l2a*, and *Isg20* in CD8$^+$ T cells (C) and CD4$^+$ T cells (D) from the HGD vs. CD groups administered an anti-PD-1 treatment.

(E) UMAP analysis of CD4$^+$ T cell subclusters from the HGD vs. CD groups administered an anti-PD-1 treatment (left), and a bar plot of the frequency of each cluster (right).

(F) Combined expression levels of cytotoxicity-related genes (*Klrk1*, *Runx3*, *Gzmb*, *Ctla2a*, *Fasl*, *Klrd1*, and *Nkg7*) with a feature plot in CD4$^+$ T cells from HGD + anti-PD-1 vs. CD + anti-PD-1 mouse groups.

(legend continued on next page)

This study suggests a new method to enhance the anti-tumor immune response against GBM, but it has several limitations. One of these limitations is that the experiments involved in this study were primarily performed using syngeneic GBM mouse models, specifically the GL261 and CT-2A models. While these models are widely accepted for GBM preclinical research, it would be valuable to investigate whether similar results are observed in spontaneous models or other alternative models. This could provide a broader understanding of the potential implications beyond the specific models employed in this study. Furthermore, it is worth noting that the number of mice utilized for the mouse models was somewhat limited. To enhance the robustness and generalizability of our findings, increasing the sample size in future studies could be considered. This would allow for a more comprehensive evaluation of the observed effects and potentially strengthen the conclusions drawn from this study.

Although the anti-tumor immune response was shown to be enhanced by HGD supplementation through various immune cell analysis methods such as scRNA-seq and flow cytometry, the mechanism that links the gut microbiota to anti-tumor immunity remains unknown. In addition, how bacteria belonging to the Desulfovibrionaceae family influence the anti-tumor immune response, particularly $CD107a^{+}NKG2D^{+}CD4^{+}$ T cells, has not yet been determined. Although members of the *Desulfovibrio* genus comprise approximately 1% of the colon microbiota, little is known about them compared to other gut microbiome flora.[49] The *Desulfovibrio* genus is closely associated with intestinal autoimmune diseases such as ulcerative colitis and Crohn disease, and the relative load of *Desulfovibrio* is increased in most colon sites in patients with ulcerative colitis.[50] Although *Desulfovibrio* is thought to be involved in the pathogenesis of inflammatory bowel disease, its role is not known.[51] The genus *Desulfovibrio* is a major producer of hydrogen sulfide (H_2S) in the gut.[52] We attempted to determine whether H_2S is a key molecule of the GBM immune modulation mechanism by supplying H_2S to the gut or by administering a chelating agent through oral gavage. However, no significant difference in survival was observed, due to the toxicity of the administered substances. Further studies of the effects of H_2S will require genetically engineered bacteria.

There is still much to learn about the effect of the gut microbiota on the anti-tumor immune response in non-inflamed cold tumors such as GBM. As a result of our studies of the effects of the gut microbiota in the GBM cold tumor model, we expect to identify key modulators of tumor growth for other tumors that do not respond to ICIs. This study demonstrated that HGD supplementation induced an increase in bacteria in the Desulfovibrionaceae family which enhanced the anti-tumor immune response to GBM. We further demonstrated that ICIs could have a synergistic effect with HGD supplementation. In conclusion, our results suggest that modulation of the gut microbiota by HGD supplementation may serve as an adjuvant to enhance the effect of ICIs. However, further studies of the role and mechanisms of *Desulfovibrio* species in anti-tumor immune modulation in GBM are needed.

STAR★METHODS

Detailed methods are provided in the online version of this paper and include the following:

- KEY RESOURCES TABLE
- RESOURCE AVAILABILITY
  - Lead contact
  - Materials availability
  - Data and code availability
- EXPERIMENTAL MODEL AND STUDY PARTICIPANT DETAILS
  - Mice
  - Tumor cell lines
  - Bacteria
- METHOD DETAILS
  - Syngeneic mouse glioblastoma model
  - Mouse treatments
  - Glucose test
  - Mouse tumor and lymph node digestion and cell isolation
  - Bacterial DNA isolation and 16S ribosomal RNA gene sequencing from fecal samples
  - Antibiotic treatment
  - *Bacterial* colonization
  - Gut permeability test
  - Flow cytometry
  - Single-cell RNA sequencing
  - Immune checkpoint blockade administration
  - Statistical analysis

SUPPLEMENTAL INFORMATION

Supplemental information can be found online at https://doi.org/10.1016/j.celrep.2023.113220.

ACKNOWLEDGMENTS

The authors thank Ji Ye Kim at the BioMedical Research Center for technical service and all members of the Host Defenses lab for thoughtful advice. This work was supported by the National Research Foundation of Korea grants NRF-2021M3A9H3015688 and NRF-2021M3A9D3026428.

AUTHOR CONTRIBUTIONS

J.K., Y.K., J.L., H.-J.K., W.H.P., K.B.K., B.H.K., S.H.P., J.L., M.S.K., and H.K.L. designed and performed the experiments. J.K. and H.K.L. conceived the

(G and H) Differences in geometric mean fluorescence intensity (gMFI) of granzyme B (G) and NKG2D (H) in the subsets of $CD4^{+}$ T cells according to CD107a expression.

(I) Frequency of $CD107a^{+}$ cells in $CD4^{+}$ T cells in the mouse GBM TME from the CD vs. HGD groups.

(J) Median survival of CD (29 days; n = 5) was compared with that of HGD (31 days; n = 5, p = 0.1241) by log-rank analysis with anti-PD-1 treatment in GBM mouse model depleted of $CD4^{+}$ T cells via an anti-mouse CD4 depletion antibody.

Survival and FACS data were obtained from two independent experiments. ns, not significant; *$p < 0.05$.

study, analyzed the data, and wrote the manuscript. H.K.L. supervised the study.

DECLARATION OF INTERESTS

The authors declare no competing interests.

INCLUSION AND DIVERSITY

We support inclusive, diverse, and equitable conduct of research.

Received: January 13, 2023
Revised: August 22, 2023
Accepted: September 20, 2023

REFERENCES

1. Michaud, C.M., Murray, C.J., and Bloom, B.R. (2001). Burden of disease–implications for future research. JAMA *285*, 535–539. https://doi.org/10.1001/jama.285.5.535.
2. Christ, A., and Latz, E. (2019). The Western lifestyle has lasting effects on metaflammation. Nat. Rev. Immunol. *19*, 267–268. https://doi.org/10.1038/s41577-019-0156-1.
3. Halton, T.L., Willett, W.C., Liu, S., Manson, J.E., Stampfer, M.J., and Hu, F.B. (2006). Potato and french fry consumption and risk of type 2 diabetes in women. Am. J. Clin. Nutr. *83*, 284–290. https://doi.org/10.1093/ajcn/83.2.284.
4. Powell, E.S., Smith-Taillie, L.P., and Popkin, B.M. (2016). Added Sugars Intake Across the Distribution of US Children and Adult Consumers: 1977-2012. J. Acad. Nutr. Diet. *116*, 1543–1550.e1. https://doi.org/10.1016/j.jand.2016.06.003.
5. Malik, V.S., and Hu, F.B. (2022). The role of sugar-sweetened beverages in the global epidemics of obesity and chronic diseases. Nat. Rev. Endocrinol. *18*, 205–218. https://doi.org/10.1038/s41574-021-00627-6.
6. Malik, V.S., Popkin, B.M., Bray, G.A., Després, J.P., and Hu, F.B. (2010). Sugar-sweetened beverages, obesity, type 2 diabetes mellitus, and cardiovascular disease risk. Circulation *121*, 1356–1364. https://doi.org/10.1161/CIRCULATIONAHA.109.876185.
7. Makarem, N., Bandera, E.V., Nicholson, J.M., and Parekh, N. (2018). Consumption of Sugars, Sugary Foods, and Sugary Beverages in Relation to Cancer Risk: A Systematic Review of Longitudinal Studies. Annu. Rev. Nutr. *38*, 17–39. https://doi.org/10.1146/annurev-nutr-082117-051805.
8. Phoomak, C., Vaeteewoottacharn, K., Silsirivanit, A., Saengboonmee, C., Seubwai, W., Sawanyawisuth, K., Wongkham, C., and Wongkham, S. (2017). High glucose levels boost the aggressiveness of highly metastatic cholangiocarcinoma cells via O-GlcNAcylation. Sci. Rep. *7*, 43842. https://doi.org/10.1038/srep43842.
9. Flores-López, L.A., Martínez-Hernández, M.G., Viedma-Rodríguez, R., Díaz-Flores, M., and Baiza-Gutman, L.A. (2016). High glucose and insulin enhance uPA expression, ROS formation and invasiveness in breast cancer-derived cells. Cell. Oncol. *39*, 365–378. https://doi.org/10.1007/s13402-016-0282-8.
10. Li, X., Li, J., Cai, Y., Peng, S., Wang, J., Xiao, Z., Wang, Y., Tao, Y., Li, J., Leng, Q., et al. (2018). Hyperglycaemia-induced miR-301a promotes cell proliferation by repressing p21 and Smad4 in prostate cancer. Cancer Lett. *418*, 211–220. https://doi.org/10.1016/j.canlet.2018.01.031.
11. Silva, C., Andrade, N., Guimarães, J.T., Patrício, E., and Martel, F. (2021). The in vitro effect of the diabetes-associated markers insulin, leptin and oxidative stress on cellular characteristics promoting breast cancer progression is GLUT1-dependent. Eur. J. Pharmacol. *898*, 173980. https://doi.org/10.1016/j.ejphar.2021.173980.
12. Cheng, H.C., Chang, T.K., Su, W.C., Tsai, H.L., and Wang, J.Y. (2021). Narrative review of the influence of diabetes mellitus and hyperglycemia on colorectal cancer risk and oncological outcomes. Transl. Oncol. *14*, 101089. https://doi.org/10.1016/j.tranon.2021.101089.
13. Ringel, A.E., Drijvers, J.M., Baker, G.J., Catozzi, A., García-Cañaveras, J.C., Gassaway, B.M., Miller, B.C., Juneja, V.R., Nguyen, T.H., Joshi, S., et al. (2020). Obesity Shapes Metabolism in the Tumor Microenvironment to Suppress Anti-Tumor Immunity. Cell *183*, 1848–1866.e26. https://doi.org/10.1016/j.cell.2020.11.009.
14. Peck, B., and Schulze, A. (2019). Lipid Metabolism at the Nexus of Diet and Tumor Microenvironment. Trends Cancer *5*, 693–703. https://doi.org/10.1016/j.trecan.2019.09.007.
15. Palmer, C.S., Cherry, C.L., Sada-Ovalle, I., Singh, A., and Crowe, S.M. (2016). Glucose Metabolism in T Cells and Monocytes: New Perspectives in HIV Pathogenesis. EBioMedicine *6*, 31–41. https://doi.org/10.1016/j.ebiom.2016.02.012.
16. Von Ah Morano, A.E., Dorneles, G.P., Peres, A., and Lira, F.S. (2020). The role of glucose homeostasis on immune function in response to exercise: The impact of low or higher energetic conditions. J. Cell. Physiol. *235*, 3169–3188. https://doi.org/10.1002/jcp.29228.
17. Tomiyama, A.J., Mann, T., Vinas, D., Hunger, J.M., Dejager, J., and Taylor, S.E. (2010). Low calorie dieting increases cortisol. Psychosom. Med. *72*, 357–364. https://doi.org/10.1097/PSY.0b013e3181d9523c.
18. Lee, Y.S., Lee, C., and Jun, H.S. (2018). Infrequent Feeding of Restricted Amounts of Food Induces Stress and Adipose Tissue Inflammation, Contributing to Impaired Glucose Metabolism. Int. J. Med. Sci. *15*, 1667–1675. https://doi.org/10.7150/ijms.28503.
19. Goncalves, M.D., Lu, C., Tutnauer, J., Hartman, T.E., Hwang, S.K., Murphy, C.J., Pauli, C., Morris, R., Taylor, S., Bosch, K., et al. (2019). High-fructose corn syrup enhances intestinal tumor growth in mice. Science *363*, 1345–1349. https://doi.org/10.1126/science.aat8515.
20. Zelenskiy, S., Thompson, C.L., Tucker, T.C., and Li, L. (2014). High dietary glycemic load is associated with increased risk of colon cancer. Nutr. Cancer *66*, 362–368. https://doi.org/10.1080/01635581.2014.884231.
21. Kiran, N., Prizment, A.E., Lazovich, D., Mao, Z., and Bostick, R.M. (2022). Sucrose Intakes and Incident Colorectal Cancer Risk among Women. J. Am. Nutraceutical Assoc. *41*, 57–63. https://doi.org/10.1080/07315724.2020.1848661.
22. Liu, L., Huh, J.R., and Shah, K. (2022). Microbiota and the gut-brain-axis: Implications for new therapeutic design in the CNS. EBioMedicine *77*, 103908. https://doi.org/10.1016/j.ebiom.2022.103908.
23. Mehrian-Shai, R., Reichardt, J.K.V., Harris, C.C., and Toren, A. (2019). The Gut-Brain Axis, Paving the Way to Brain Cancer. Trends Cancer *5*, 200–207. https://doi.org/10.1016/j.trecan.2019.02.008.
24. Liang, J., Li, T., Zhao, J., Wang, C., and Sun, H. (2022). Current understanding of the human microbiome in glioma. Front. Oncol. *12*, 781741. https://doi.org/10.3389/fonc.2022.781741.
25. Morais, L.H., Schreiber, H.L., 4th, and Mazmanian, S.K. (2021). The gut microbiota-brain axis in behaviour and brain disorders. Nat. Rev. Microbiol. *19*, 241–255. https://doi.org/10.1038/s41579-020-00460-0.
26. Gonzalez-Santana, A., and Diaz Heijtz, R. (2020). Bacterial Peptidoglycans from Microbiota in Neurodevelopment and Behavior. Trends Mol. Med. *26*, 729–743. https://doi.org/10.1016/j.molmed.2020.05.003.
27. Zmora, N., Suez, J., and Elinav, E. (2019). You are what you eat: diet, health and the gut microbiota. Nat. Rev. Gastroenterol. Hepatol. *16*, 35–56. https://doi.org/10.1038/s41575-018-0061-2.
28. Zhu, S., Jiang, Y., Xu, K., Cui, M., Ye, W., Zhao, G., Jin, L., and Chen, X. (2020). The progress of gut microbiome research related to brain disorders. J. Neuroinflammation *17*, 25. https://doi.org/10.1186/s12974-020-1705-z.
29. Gopalakrishnan, V., Spencer, C.N., Nezi, L., Reuben, A., Andrews, M.C., Karpinets, T.V., Prieto, P.A., Vicente, D., Hoffman, K., Wei, S.C., et al. (2018). Gut microbiome modulates response to anti-PD-1 immunotherapy in melanoma patients. Science *359*, 97–103. https://doi.org/10.1126/science.aan4236.

30. Zheng, Y., Wang, T., Tu, X., Huang, Y., Zhang, H., Tan, D., Jiang, W., Cai, S., Zhao, P., Song, R., et al. (2019). Gut microbiome affects the response to anti-PD-1 immunotherapy in patients with hepatocellular carcinoma. J. Immunother. Cancer *7*, 193. https://doi.org/10.1186/s40425-019-0650-9.

31. Matson, V., Fessler, J., Bao, R., Chongsuwat, T., Zha, Y., Alegre, M.L., Luke, J.J., and Gajewski, T.F. (2018). The commensal microbiome is associated with anti-PD-1 efficacy in metastatic melanoma patients. Science *359*, 104–108. https://doi.org/10.1126/science.aao3290.

32. Sivan, A., Corrales, L., Hubert, N., Williams, J.B., Aquino-Michaels, K., Earley, Z.M., Benyamin, F.W., Lei, Y.M., Jabri, B., Alegre, M.L., et al. (2015). Commensal Bifidobacterium promotes antitumor immunity and facilitates anti-PD-L1 efficacy. Science *350*, 1084–1089. https://doi.org/10.1126/science.aac4255.

33. Routy, B., Le Chatelier, E., Derosa, L., Duong, C.P.M., Alou, M.T., Daillère, R., Fluckiger, A., Messaoudene, M., Rauber, C., Roberti, M.P., et al. (2018). Gut microbiome influences efficacy of PD-1-based immunotherapy against epithelial tumors. Science *359*, 91–97. https://doi.org/10.1126/science.aan3706.

34. Liu, Z.G., and Jiao, D. (2019). Necroptosis, tumor necrosis and tumorigenesis. Cell stress *4*, 1–8. https://doi.org/10.15698/cst2020.01.208.

35. Houston, S.A., Cerovic, V., Thomson, C., Brewer, J., Mowat, A.M., and Milling, S. (2016). The lymph nodes draining the small intestine and colon are anatomically separate and immunologically distinct. Mucosal Immunol. *9*, 468–478. https://doi.org/10.1038/mi.2015.77.

36. Thaiss, C.A., Levy, M., Grosheva, I., Zheng, D., Soffer, E., Blacher, E., Braverman, S., Tengeler, A.C., Barak, O., Elazar, M., et al. (2018). Hyperglycemia drives intestinal barrier dysfunction and risk for enteric infection*359*, pp. 1376–1383. https://doi.org/10.1126/science.aar3318.

37. Zhou, C.B., Zhou, Y.L., and Fang, J.Y. (2021). Gut Microbiota in Cancer Immune Response and Immunotherapy. Trends Cancer *7*, 647–660. https://doi.org/10.1016/j.trecan.2021.01.010.

38. Zitvogel, L., Ma, Y., Raoult, D., Kroemer, G., and Gajewski, T.F. (2018). The microbiome in cancer immunotherapy: Diagnostic tools and therapeutic strategies. Science *359*, 1366–1370. https://doi.org/10.1126/science.aar6918.

39. Zhang, J., Huang, D., Saw, P.E., and Song, E. (2022). Turning cold tumors hot: from molecular mechanisms to clinical applications. Trends Immunol. *43*, 523–545. https://doi.org/10.1016/j.it.2022.04.010.

40. Zhou, Y., Liu, Z., and Chen, T. (2022). Gut Microbiota: A Promising Milestone in Enhancing the Efficacy of PD1/PD-L1 Blockade Therapy. Front. Oncol. *12*, 847350. https://doi.org/10.3389/fonc.2022.847350.

41. Vreman, R.A., Goodell, A.J., Rodriguez, L.A., Porco, T.C., Lustig, R.H., and Kahn, J.G. (2017). Health and economic benefits of reducing sugar intake in the USA, including effects via non-alcoholic fatty liver disease: a microsimulation model. BMJ Open *7*, e013543. https://doi.org/10.1136/bmjopen-2016-013543.

42. Goncalves, M.D., Hopkins, B.D., and Cantley, L.C. (2019). Dietary Fat and Sugar in Promoting Cancer Development and Progression. Annu. Rev. Cell Biol. *3*, 255–273. https://doi.org/10.1146/annurev-cancerbio-030518-055855.

43. Capitani, N., Patrussi, L., and Baldari, C.T. (2021). Nature vs. Nurture: The Two Opposing Behaviors of Cytotoxic T Lymphocytes in the Tumor Microenvironment. Int. J. Mol. Sci. *22*, 11221. https://doi.org/10.3390/ijms222011221.

44. Tay, R.E., Richardson, E.K., and Toh, H.C. (2021). Revisiting the role of CD4(+) T cells in cancer immunotherapy-new insights into old paradigms. Cancer Gene Ther. *28*, 5–17. https://doi.org/10.1038/s41417-020-0183-x.

45. Laidlaw, B.J., Craft, J.E., and Kaech, S.M. (2016). The multifaceted role of CD4(+) T cells in CD8(+) T cell memory. Nat. Rev. Immunol. *16*, 102–111. https://doi.org/10.1038/nri.2015.10.

46. Stojanovic, A., Correia, M.P., and Cerwenka, A. (2018). The NKG2D/NKG2DL Axis in the Crosstalk Between Lymphoid and Myeloid Cells in Health and Disease. Front. Immunol. *9*, 827. https://doi.org/10.3389/fimmu.2018.00827.

47. Juno, J.A., van Bockel, D., Kent, S.J., Kelleher, A.D., Zaunders, J.J., and Munier, C.M.L. (2017). Cytotoxic CD4 T Cells-Friend or Foe during Viral Infection? Front. Immunol. *8*, 19. https://doi.org/10.3389/fimmu.2017.00019.

48. Oh, D.Y., and Fong, L. (2021). Cytotoxic CD4(+) T cells in cancer: Expanding the immune effector toolbox. Immunity *54*, 2701–2711. https://doi.org/10.1016/j.immuni.2021.11.015.

49. Dordević, D., Jančíková, S., Vítězová, M., and Kushkevych, I. (2021). Hydrogen sulfide toxicity in the gut environment: Meta-analysis of sulfate-reducing and lactic acid bacteria in inflammatory processes. J. Adv. Res. *27*, 55–69. https://doi.org/10.1016/j.jare.2020.03.003.

50. Loubinoux, J., Bronowicki, J.P., Pereira, I.A.C., Mougenel, J.L., and Faou, A.E. (2002). Sulfate-reducing bacteria in human feces and their association with inflammatory bowel diseases. FEMS Microbiol. Ecol. *40*, 107–112. https://doi.org/10.1111/j.1574-6941.2002.tb00942.x.

51. Kushkevych, I., Dordević, D., and Kollár, P. (2018). Analysis of Physiological Parameters of Desulfovibrio Strains from Individuals with Colitis. Open Life Sci. *13*, 481–488. https://doi.org/10.1515/biol-2018-0057.

52. Ijssennagger, N., van der Meer, R., and van Mil, S.W.C. (2016). Sulfide as a Mucus Barrier-Breaker in Inflammatory Bowel Disease? Trends Mol. Med. *22*, 190–199. https://doi.org/10.1016/j.molmed.2016.01.002.

STAR★METHODS

KEY RESOURCES TABLE

REAGENT or RESOURCE	SOURCE	IDENTIFIER
Antibodies		
anti-mouse CD45.2-AF700 (Clone: 104)	BioLegend	Cat# 109822; RRID: AB_493731
anti-mouse CD45.2-eF450 (Clone: 104)	eBioscience	Cat# 48-0454-82; RRID: AB_11042125
anti-mouse CD3ε-PE-Cy7 (Clone: 145-2C11)	BD Biosciences	Cat# 552774; RRID: AB_394460
anti-mouse CD11b-Bv510 (Clone: M1/70)	BD Biosciences	Cat# 562950; RRID: AB_2737913
anti-mouse GZMB-FITC (Clone: NGZB)	eBioscience	Cat# 11-8898-82; RRID: AB_10733414
anti-mouse IFN-γ-PE (Clone: XMG1.2)	BioLegend	Cat# 505808; RRID: AB_315402
anti-mouse NKG2D-PE-Cy7 (Clone: CX5)	eBioscience	Cat# 25-5882-81; RRID: AB_469656
anti-mouse CD4-PerCP-Cy5.5 (Clone: RM4-5)	BD Bioscience	Cat# 550954; RRID: AB_393977
anti-mouse CD4-BV421 (Clone: GK1.5)	eBioscience	Cat# 48-0041-82; RRID: AB_10718983
anti-mouse CD44-PerCP-Cy5.5 (Clone: IM7)	Biolegend	Cat# 103032; RRID: AB_2076204
anti-mouse CD62L-PE (Clone: MEL-14)	BD Biosciences	Cat# 553152; RRID: AB_398533
anti-mouse CD107a-APC (Clone: 1D4B)	BioLegend	Cat# 121614; RRID: AB_2234505
anti-mouse TNF-α-APC-Cy7 (Clone: MP6-XT22)	BioLegend	Cat# 506343; RRID: AB_2565952
anti-mouse CD8-Bv510 (Clone: 53–6.7)	BD Biosciences	Cat# 563068; RRID: AB_2687548
anti-mouse CD45.2-PerCP-Cy5.5 (Clone: 104)	BD Biosciences	Cat# 552950; RRID: AB_394528
anti-mouse CD45.2-APC (Clone: 104)	BD Biosciences	Cat# 558702; RRID: AB_1645215
anti-mouse NK1.1-PE (Clone: PK136)	BioLegend	Cat# 108708; RRID: AB_313395
anti-mouse FOXP3-APC (Clone: FJK-16s)	eBioscience	Cat# 17-5773-82; RRID: AB_467576
anti-mouse CD3ε-APC-Cy7 (Clone: 17A2)	BioLegend	Cat# 100222; RRID: AB_2242784
FITC-Rat IgG2a, κ (Clone: eBR2a)	eBioscience	Cat# 11-4321-42; RRID: AB_10669580
PE-Cy7-Rat IgG2a, κ (Clone: R35-95)	BD Biosciences	Cat# 552784; RRID: AB_394465
PE-Rat IgG1, κ (Clone: A19-3)	BD Biosciences	Cat# 555749; RRID: AB_396091
APC-Rat IgG2a, κ (Clone: RTK2758)	BioLegend	Cat# 400511; RRID: AB_2814702
APC-Cy7-Rat IgG1, κ (Clone: RTK2071)	BioLegend	Cat# 400422; RRID: AB_830905
Anti-CD16/32 (Clone: 2.4G2; Fc blocker)	Lab generated	N/A
InVivoMAb anti-mouse CD8 (Clone: 2.43)	Bio X Cell	Cat# BE0061; RRID: AB_1125541
InVivoMAb anti-mouse CD4 (Clone: GK1.5)	Bio X Cell	Cat# BE0003-1; RRID: AB_1107636
InVivoMAb rat IgG2b isotype control (Clone: LTF-2)	Bio X Cell	Cat# BE0090; RRID: AB_1107780
InVivoMAb anti-mouse PD-1 (CD279) (Clone: RMP1-14)	Bio X Cell	Cat# BE0146; RRID: AB_10949053
InVivoMAb rat IgG2a isotype control, anti-trinitrophenol (Clone: 2A3)	Bio X Cell	Cat# BE0089; RRID: AB_1107769
Bacterial and virus strains		
Desulfovibrio vulgaris	KCTC	2360
Desulfovibrio desulfuricans	KCTC	5768
Faecalubaculum rodentium	KCTC	15484
Alistipes shahii	KCTC	15238
Chemicals, peptides, and recombinant proteins		
Dextrose anhydrous	Daejung	Cat# 3020-4400
Dulbecco's phosphate-buffered saline	Corning	Cat# 21-031-CVC
Dulbecco's Modified Eagle Medium	Corning	Cat# 10-013-CVRC
Fetal bovine serum, premium, United States origin	Corning	Cat# 35-015-CV

(*Continued on next page*)

Continued

REAGENT or RESOURCE	SOURCE	IDENTIFIER
Bovine Serum	Gibco	16140–078
Penicillin-streptomycin (100X)	GenDEPOT	CA-005-010
Trypsin-EDTA solution (0.5 M)	Welgene	ML005-01
RPMI1640	Corning	10-040-CVRC
Propidium Iodide solution	BioLegend	421302
7-AAD	BioLegend	420404
Percoll	GE Healthcare	17-0891-01
HBSS (with phenol red and sodium bicarbonate, without calcium chloride and magnesium sulfate)	Welgene	LB003-03
Collagenase IV	Worthington	LS004189
DNase I	Roche	10104159001
Ampicillin	AG Scientific	Cat# A-1414
Vancomycin	AG Scientific	Cat# V-1065
Neomycin sulfate	AG Scientific	Cat# N-1053
Gentamycin	AG Scientific	Cat# G-1067
Metronidazole	Sigma	Cat# M1547-25G
Phorbol 12-myristate 13-acetate	Sigma	Cat# P1085
Ionomycin calcium salt	Sigma	Cat# I3909
GolgiStop protein transport inhibitor (monensin)	BD Biosciences	Cat# 554724
GolgiPlug protein transport inhibitor (Brefeldin A)	BD Biosciences	Cat# 555029
Cytofix/Cytoperm fixation and permeabilization solution	BD Biosciences	Cat# 554722
FOXP3 Fix/Perm Buffer set	BioLegend	Cat# 421403
Zombie Aqua Fixable Viability Kit	BioLegend	Cat# 423101
Fixable viability dye 450	eBioscience	Cat# 65-0863-14
Fixable viability stain 780	BD Biosciences	Cat# 565388
Tryptic soy broth	Difco	Cat# 211825
Defibrinated sheep blood	KisanBio	Cat# MB-S1876
Fluorescein isothiocyanate–dextran mol wt 3,000–5,000	Sigma	SIG-FD4-1G
Critical commercial assays		
QIAamp DNA Stool Mini Kit	QIAGEN	Cat# 51604
Chromium Single Cell 3′ reagent Kits v3	10X Genomics	N/A
Agilent High Sensitivity DNA kit	Agilent	5067–4626
HiSeq X Ten Reagent Kit v2.5	Illumina	FC-501-2501
PhiX Control v3	Illumina	FC-110-3001
SPRIselect Reagent Kit	Beckman Coulter	B23318
eMyco plus Mycoplasma PCR Kit	iNtRON Biotechnology	Cat# 25237
Deposited data		
scRNAseq raw data	This manuscript	GEO: GSE222192
Experimental models: Cell lines		
Mouse: GL261	Dr. Injun Kim (KAIST)	N/A
Mouse: GL261-GFP	Dr. Injun Kim (KAIST)	N/A
Mouse: CT-2A	Merck Millipore	Cat# SCC194

(*Continued on next page*)

Continued

REAGENT or RESOURCE	SOURCE	IDENTIFIER
Experimental models: Organisms/strains		
Mouse: C57BL/6J	KAIST	https://spf.kaist.ac.kr/
Mouse: C57BL/6J	DBL. Co. Ltd	http://www.dbl.kr/bbs/board.php?tbl=animal&chr=&category=%2C%27DBL+%EC%83%9D%EC%82%B0%EB%8F%99%EB%AC%BC%27&findType=&findWord=&sort1=&sort2%20=%20
Mouse: Germ-free C57BL/6J	POSTECH	https://biotechcenter.org/06_labanimal/labanimal01.html#link2
Mouse: NOD/Shi-scid, IL-2Rγnull	KOATECH	http://www.koatech.co.kr/sub02/01.php#
Oligonucleotides		
Desulfovibrio PCR primers Forward: 5′-CCGTAGATATCTGGAGGAA CATCAG-3′	(Fite et al. 2004)	https://doi.org/10.1128/AEM.02851-10
Desulfovibrio PCR primers Reverse: 5′-ACATCTAGCATCCATCGTT TACAGC-3′	(Fite et al. 2004)	https://doi.org/10.1128/AEM.02851-10
Software and algorithms		
EzBioCloud 16S rRNA database	CJ Bioscience	https://www.ezbiocloud.net/
R statistical programming environment v. 4.2.1	R Core	https://www.r-project.org
Cell Ranger 3.1.0	10X Genomics	
R studio		https://rstudio.com
Seurat_4.1.0	(Hao et al., 2021)	https://satijalab.org/seurat/
GSEA software v.4.0.3	GSEA	https://www.gsea-msigdb.org
FlowJo v.10.5.3	Treestar	https://www.flowjo.com/solutions/flowjo/downloads
Prism software v.9.0	Graphpad	https://www.graphpad.com/scientific-software/prism/
Other		
CellDropTM Automated Cell Counter	DeNovix	CellDrop FL-UNLTD
Digital mouse stereotaxic frame	World Precision Instruments	505314
Animal Anesthesia Vaporizers type 1	RWD	R580S
Syringe Pump	KD Scientific	LEGATO 130
Hamilton Syringe	Hamilton	803
Reflex 7mm wound clips	Roboz	RS-9258
Accu-chek active device	Roche Diabetes Care GmbH	6013410520505
HiSeq X Ten	Illumina	N/A
MiniAmp Thermal Cycler	Thermo Fisher Scientific	A37834
Chromium Controller	10X	N/A
2100 Bioanalyzer	Agilent	G2939BA
LSRFortessa^{TM} X-20 Cell Analyzer	BD Biosciences	N/A
FACSAria II	BD Biosciences	N/A
Micro Drill	SAESHIN	N/A
Oral zoned needle	JEUNG DO B&P	JD-S-124
Petroff-Hauser chamber	Fisher Scientific	267113

RESOURCE AVAILABILITY

Lead contact

Requests for resources, reagents, and further information should be directed to the lead contact, Heung Kyu Lee (heungkyu.lee@kaist.ac.kr).

Materials availability

All mouse lines and materials used in this study were provided or purchased from mentioned companies or researchers. This study did not generate any new or unique reagents.

Data and code availability

- Single-cell RNA sequencing data GSE222192 from SPF mice supplemented with CD and HGD, GF mice supplemented with CD and HGD, and mice supplemented with CD and HGD and treated with anti-PD-1 is deposited and publicly available in the Gene Expression Omnibus (GEO) at National Center for Biotechnology Information (NCBI).
- This paper does not report original code.
- Any additional information required to reanalyze the data reported in this paper is available from the lead contact upon request.

EXPERIMENTAL MODEL AND STUDY PARTICIPANT DETAILS

Mice

Specific pathogen-free (SPF) male C57BL/6J mice between 8 and 12 weeks of age at the time of GL261 tumor implantation were used. Unless otherwise noted, all mice were bred in an SPF facility of the Korea Advanced Institute of Science and Technology (KAIST, Daejeon, Korea) Laboratory Animal Resource Center with no more than five mice per cage. C57BL/6J mice were purchased from KAIST and DBL Co. Ltd (Eumseong, Korea). GF mice were purchased from POSTECH Biotechnology Research Center (Pohang, Korea). NOD/Shi-scid, IL-2Rγnull (NOG) immunodeficient mice were purchased from KOATECH (Pyeongtaek, Korea). All procedures were performed according to the guidelines and protocols of KAIST's Institutional Animal Care and Use Committee (IACUC) and were approved by the IACUC.

Tumor cell lines

The GL261 mouse glioma cell lines and GFP-expressing GL261 (GL261-GFP) cell lines were provided by Professor Injun Kim of KAIST. We purchased the CT-2A mouse glioma cell line (Sigma-Aldrich, St. Louis, MO, USA). The mouse tumor cell line was cultured in a cell culture flask with 1% penicillin/streptomycin (GenDEPOT, USA) and 10% fetal bovine serum (Corning, NY, USA) added to Dulbecco's Modified Eagle Medium (DMEM, Corning, NY, USA) at 37°C with 5% CO_2. The absence of mycoplasma contamination was confirmed in the cell line used for the experiment using a Mycoplasma PCR kit (Intron Biotechnology, Seongnam, Korea). Cells were dissociated using trypsin-ethylenediaminetetraacetic acid (EDTA) (Corning).

Bacteria

Desulfovibrio vulgaris, *Faecalubaculum rodentium*, and *Alistipes shahii* were used to colonize the mouse colon microbiome and were purchased from Korean Collection for Type Cultures (KCTC, Korea). For bacterial cultures, 30 g of tryptic soy broth (Bacto Tryptic Soy Broth, Difco, 211825) was resuspended in one liter of distilled water and then sealed and autoclaved. After the temperature decreased to 50°C or less, 50 mL of defibrinated sheep blood (KisanBio, MB-S1876) was added to prepare the broth for culturing.

METHOD DETAILS

Syngeneic mouse glioblastoma model

To induce GBM in the mouse brain, we used an orthotopic glioma injection model by inoculating the brain with the mouse glioma cell lines mentioned above. Each mouse was implanted with 2×10^5 GL261 cells. GL261 cells were removed from the cell culture flask using trypsin-EDTA, neutralized with DMEM, and then washed with Dulbecco's phosphate-buffered saline (DPBS). Cells were diluted to 10^5 cells/μl in DPBS and stored on ice until inoculation in the brain.

For inoculation, the mouse was placed on a heating plate at 37°C to maintain body temperature after the administration of inhalation anesthesia. After the head was fixed in a stereotactic device (Stoelting Co, Wood Dale, IL, USA), an ophthalmic ointment was applied to the eyes to protect them from dryness and damage. After sterilizing the scalp by applying povidone, a midline incision was made in the skin covering the top of the skull. Then, the skin was opened to expose the skull, and a hole was drilled in the skull 2 mm to the right and 2 mm anterior from the bregma using a stereotactic instrument. The prepared GL261 or CT-2A cells were loaded into a Hamilton syringe (The Hamilton Company, Reno, NV, USA) and injected for 5 min at a rate of 0.4 μL/min with a nano-injector (KD Scientific, Holliston, MA, USA) into the hole made by the drill at a depth of 3 mm from the brain surface. Total of 2×10^5 cells were inoculated. After the injection, the skull hole was closed with adhesive, and the skin was sutured using a 7-mm wound clip (Roboz, Gaithersburg, MD, USA). The incision site was again sterilized with povidone, and oxygen was supplied while the mouse recovered on a heating pad.

Mouse treatments

To alter the gut microbiota, we dissolved dextrose in distilled water (20% final concentration) (dextrose anhydrous, Daejung, Korea) and loaded it into a water bottle. For the HGD experimental model, we supplied mice with 20% dextrose water for 5 weeks before and

2 weeks after tumor cell inoculation. To prevent spoilage, we changed water bottles twice a week, and 20% dextrose water was freshly prepared and supplied each time.

For $CD4^+$ and $CD8^+$ T cell depletion, 150 μg of an InVivoMab anti-mouse CD4 depletion antibody (BioXcell, Clone: GK1.5) and an InVivoMab anti-mouse CD8 depletion antibody (BioXcell, Clone: 2.43) were diluted in 200 μL of DPBS and injected intraperitoneally into each mouse. Intraperitoneal injection was performed 1 day before GL261 tumor injection, with additional injections 7 days and 14 days later.

Glucose test

Blood glucose levels in mice were measured using an Accu-chek Active device (Roche Diabetes Care GmbH, Germany). After the HGD or CD (control) was administered to mice for 5 weeks, the tail vein area was disinfected with an alcohol swab, and bleeding was induced by needle puncture. The blood glucose level was measured by loading the blood onto the reading spot of the device. The median of two values was recorded for each measurement. Random blood glucose levels were measured twice in the daytime, and the mean values were utilized for analysis. The fasting glucose level was measured by the same method after moving the mice to a new cage without water or food and inducing a fasting state for more than 4 h.

Mouse tumor and lymph node digestion and cell isolation

To isolate single cells from the mouse GBM TME immediately after euthanasia via a CO_2 gas chamber, we perfused 30 mL of cold DPBS solution through the heart to prevent blood contamination in the brain as much as possible. Then, only the right hemisphere, in which the cancer cells were inoculated, was extracted. The hemisphere was divided into small pieces using a blade and digested with 2 mg/mL collagenase IV (Worthington Biochemical Corporation, Columbus, OH, USA) and 30 μg/mL DNase I (Roche, Basel, Switzerland) at 37°C for 30 min in a shaking incubator. Next, the tissues were filtered through a 70-μm strainer. To isolate immune cells, we resuspended the filtered cells in 5 mL of 30% Percoll solution (GE Healthcare, Chicago, IL) containing DMEM CM and then a 70% Percoll solution containing DPBS supplemented with 1% bovine serum (Thermo Fisher Scientific) was added slowly to the bottom, followed by centrifugation at room temperature for 20 min without applying a brake. After removing the immune cells at the interface of the two Percoll layers, the cells were incubated in ACK lysis buffer at room temperature for 5 min to remove the remaining red blood cells, and further analysis was performed. For mesenteric lymph node cells, we dissected mesenteric lymph nodes from the mouse immediately after euthanasia and the lymph node tissue was digested by same protocol above mentioned. The tissue was filtered through a 70-μm strainer, and the cells were incubated in ACK lysis buffer at room temperature for 5 min to remove the remaining red blood cells, and further analysis was performed.

Bacterial DNA isolation and 16S ribosomal RNA gene sequencing from fecal samples

To identify the gut microbiota, we sequenced bacterial 16S ribosomal RNA genes from mouse feces. To obtain fresh mouse feces, we separated the mice into individual spaces and collected feces while we observed the mice for 30 min. Next, DNA was extracted from the feces according to the recommended protocol using a QIAamp DNA Mini Kit (QIAGEN, 56304). and sent to CJ Bioscience (Seoul, Korea) for sequencing the 16S rRNA genes, and the final data were analyzed using the 16S rRNA gene sequencing analysis tool provided by the EzBioCloud platform (CJ Bioscience).

Antibiotic treatment

To deplete the gut microbiota, we prepared and loaded an antibiotic cocktail containing neomycin sulfate (500 mg/L), metronidazole (500 mg/L), gentamycin (500 mg/L), ampicillin (500 mg/L), and vancomycin (250 mg/L) in distilled water into a water bottle. Mice were supplied with this solution for 2 weeks unless otherwise specified. The water bottle was replaced with a freshly prepared antibiotic cocktail every week. After 2 weeks, the mice were sacrificed, and an enlarged cecum indicated an effect of the treatment on the intestines. Bacterial colonization was induced through oral gavage 24 h after stopping antibiotic supplementation.

Bacterial colonization

For colonization, *Desulfovibrio vulgaris* and other species were cultured as described above. After culturing in broth for 3 days, bacteria were aliquoted in a medium containing 10% glycerol and stored at −80°C. Identification of *Desulfovibrio* species was confirmed through polymerase chain reaction assays (Fite et al., 2004). The forward primer was DSV691-F: 5′-CCGTAGATATCTGGAGGAA CATCAG-3′, and the reverse primer was DSV826-R: 5′-ACATCTAGCATCCATCGTTTACAGC-3′. After inserting the tube for oral gavage, a bacterial count was performed using a Petroff-Hauser chamber (Fisher Scientific, 267113). The mixture was diluted to 1×10^8 cells/100 μL of DPBS and used immediately for oral gavage. Colonization through oral gavage was performed three times a week for 2 weeks before and after GL261 tumor inoculation; 100 μL of the solution was administered to each mouse, and 100 μL of DPBS was administered to the control group.

Gut permeability test

To measure gut permeability, we maintained mice fasted without food or bedding for 4 h and then administered 4 kDa-fluorescein isothiocyanate–dextran (FITC-dextran) via oral gavage at a dose of 10 mg/125 μL per mouse. After an additional 4 h, we euthanized the mice via a CO_2 gas chamber and immediately collected blood from the heart. Following this, we performed centrifugation to

obtain plasma from the blood. The obtained plasma was diluted with DPBS at a 1:5 ratio, and the fluorescence was measured by a spectrophotometer.

Flow cytometry

Single cells were isolated as previously described. The single-cell suspensions were treated with an anti-CD16/32 antibody (2.4G2) to block Fc receptors prior to staining with mouse-specific antibodies against the following surface molecules: CD45.2 (clone: 104), CD3e (clone: 145-2C11), CD11b (clone: M1/70), CD4 (clone: RM4.5), CD8 (clone: 53–6.7), CD44(clone: IM7), CD62L(clone: MEL-14), and NKG2D (clone: CX5). Propidium iodide (00-6990-50, eBioscience) or 7-aminoactinomycin (7-AAD) (51-68981E, BD) was used to gate live cells. To stimulate tumor-derived immune cells, we cultured single-cell suspensions in RPMI complete medium with 50 ng/mL phorbol-myristate acetate (PMA, Sigma), 1 μg/mL ionomycin (Sigma), 1 μM GolgiStop (BD), and 1 μM GolgiPlug (BD) for 4 h at 37°C. Before intracellular staining, immune cell suspensions were stained with anti-mouse CD4, CD8, CD11b, and CD45.2 antibodies before fixation and permeabilization using the FOXP3 Fix/Perm Buffer Set (Biolegend) according to the manufacturer's recommended protocol. Antibodies against the following proteins were used: IFN-γ (clone: XMG1.2), CD107a (clone: ID4B), GZMB (clone: NGZB), and TNF-α (clone: MP6-XT22). Live-cell-gated staining was performed with Fixable Viability Dye eFluor 450 (65-0863-14, Thermo Fisher Scientific), Fixable Viability Strain 780 (565388, BD), or a Zombie Aqua Fixable Viability Kit (432101, Biolegend). All samples were acquired using an LSRFortessa flow cytometer (BD), and the data were analyzed using FlowJo software 10.5.3 (Treestar).

Single-cell RNA sequencing

The GL261 mouse GBM syngeneic model for mice on a CD or an HGD, as described above, was used for scRNA-seq. On day 20 following the GL261 injection, single-cell suspensions were prepared from the brain as described above. Suspensions were pooled into one sample from three mice in each group with median percentile weight of five mice. The single-cell suspensions were treated with an anti-CD16/32 antibody (2.4G2, Fc blocker) to block Fc receptors prior to staining with mouse-specific antibodies. The cells were then stained with CD45.2 (clone: 104, Biolegend). Live immune cells were isolated using a FACS Aria II (BD Biosciences) flow cytometer, and 7-AAD staining was performed before data acquisition to eliminate dead cells. For GL261 mouse tumor cell analysis *in vivo*, we used GL261-GFP cell lines for tumor inoculation and sorted tumor cells with GFP^+ and $CD45.2^-$ cells with same protocol mentioned above. A Chromium Single Cell 3′ Reagent kit (version 3; 10X Genomics) was used for scRNA-seq according to the manufacturer's recommended protocol, as previously described. Sorted cells were loaded with gel beads for emulsion generation and barcoding, cDNA was amplified, and libraries were constructed. Next-generation sequencing was performed with the HiSeqXten (Illumina) platform for 10,000 cells per pooled sample. The sequencing results were converted into FASTQ files using Cell Ranger (10X Genomics), and sequences were aligned using the mouse genome 10–3.0.0 (10X Genomics) as a reference.

Matrices were loaded into Seurat v.4.1 for analysis, and R 4.2.1 was used for statistical analysis. Cells with unique RNA features (<2.5% or >97.5% percentile of expressed genes) were excluded for quality control. Cells in which more than 5% of reads aligned to mitochondrial genes were also excluded. The data were normalized using the NormalizeData function. Changes in gene expression were identified using the FindVariableFeatures function. Datasets for the CD and HGD groups were integrated using the FindIntegrationAnchors and IntegrateData functions. The data dimension was reduced using principal component (PC) analysis for each sample, and 20 significant PCs were identified. Data were clustered using the FindNeighbors and FindClusters functions at a resolution of 0.5. RunUMAP functions were used to visualize the selected PCs. The Seurat workflow was used to sort and visualize the normalized number of genes per cell. Cluster markers were identified using the FindMarkers functions. For GSEA, DEGs were annotated on the reference gene set based on MSigDB 7.0.

Immune checkpoint blockade administration

For anti-PD-1 ICI administration, 200 μg of an InVivoMab anti-mouse PD-1 blocking antibody (BioXcell, RMP1-14) was diluted in 100 μL of DPBS and injected intraperitoneally into each mouse on days 9, 12, and 15 after GL261 tumor inoculation. As a control, an InVivoMab rat IgG2a isotype antibody (BioXcell, Clone: 2A3) at the same concentration was injected.

Statistical analysis

All data are expressed as the mean ± standard error of the mean (SEM). Statistical analyses of differences between the two groups used an unpaired, two-tailed Student's t-test. A comparison of survival rate was made with the log rank test. Prism 9.3.1 software (GraphPad, San Diego, CA, USA) was used for the statistical analysis. Statistically significant differences are indicated as follows: ns, not significant, *$p < 0.05$, **$p < 0.01$, ***$p < 0.001$, and ****$p < 0.0001$.

Cell Reports, Volume *42*

Supplemental information

Supplementation with a high-glucose drink stimulates anti-tumor immune responses to glioblastoma via gut microbiota modulation

Jaeho Kim, Yumin Kim, Jeongwoo La, Won Hyung Park, Hyun-Jin Kim, Sang Hee Park, Keun Bon Ku, Byeong Hoon Kang, Juhee Lim, Myoung Seung Kwon, and Heung Kyu Lee

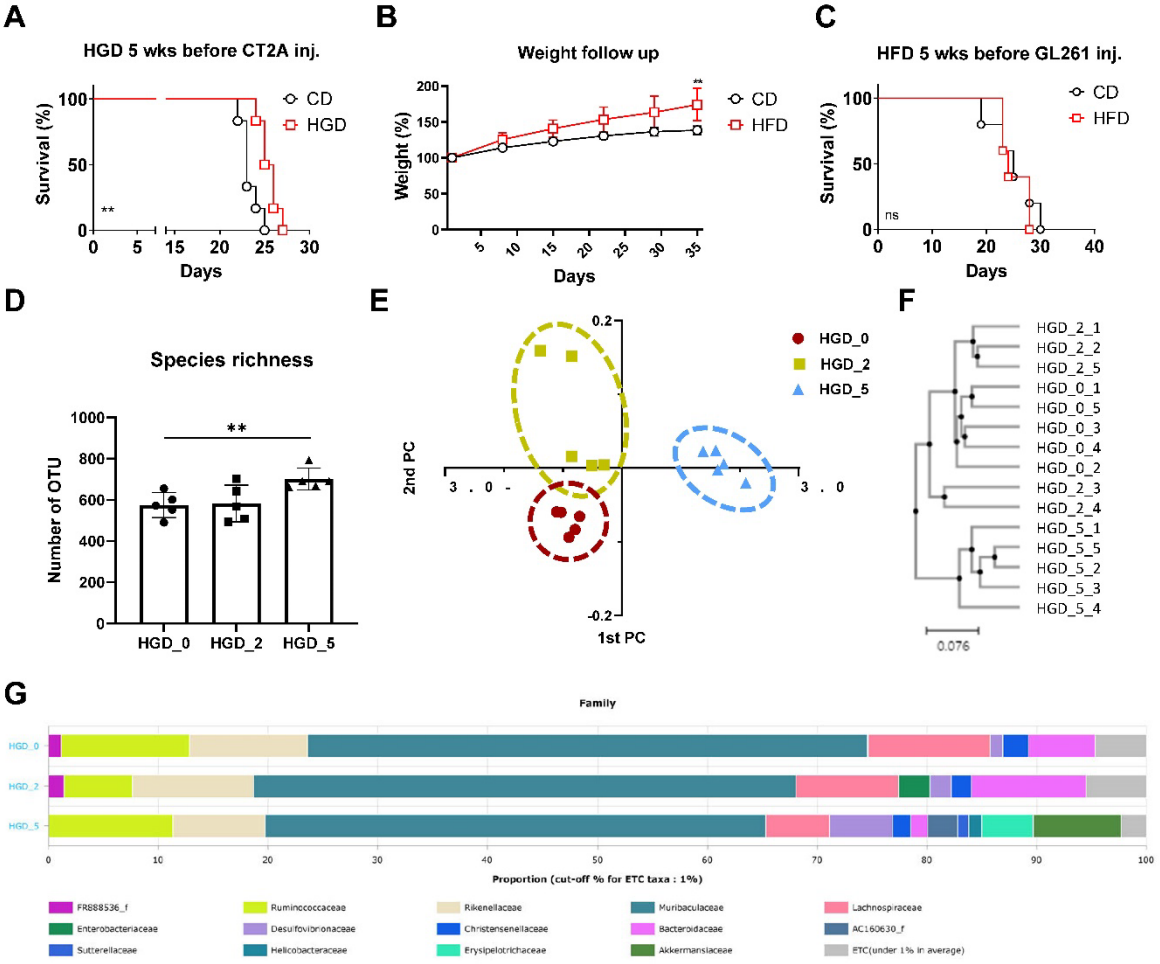

Figure S1. Supplementation with a high-glucose drink (HGD) improved the survival rate in a glioblastoma (GBM) mouse model through the gut microbiota, and a period of 5 weeks of HGD supplementation was needed for significant changes in the gut microbiota, Related to Figure 1.

(A) Median survival of mice supplied with control drink (CD) (23 days; n = 6) was compared with HGD (25.5 days; n = 6, p = 0.0084) for 5 weeks prior to the injection (inj) of CT-2A mouse glioma tumor cells by log-rank analysis.

(B) Weight of GBM model mice fed a CD or a high-fat diet (HFD) for 5 weeks and (C) median survival of mice supplied with control diet (25 days; n = 5) was compared with HGD (24 days; n = 5, p = 0.1215) for 10 weeks prior to injection of GL261 mouse glioma tumor cells by log-rank analysis.

(D) Alpha diversity of gut microbiota species richness by operational taxonomic unit (OTU) analysis in terms of the period of HGD supplementation: 0 weeks (HGD_0, n = 5), 2 weeks (HGD_2, n = 5), and 5 weeks (HGD_5, n = 5).

(E) Principal coordinates analysis (PCoA) plot and (F) unweighted pair group method with arithmetic mean (UPGMA) clustering analysis of the gut microbiota in terms of the period of HGD supplementation: 0 weeks (HGD_0, n = 5), 2 weeks (HGD_2, n = 5), and 5 weeks

(HGD_5, n = 5). (G) The relative ratios of the bacterial families in the consortia.
ns, not significant; $*p < 0.05$, $**p < 0.01$, $***p < 0.001$, $****p < 0.0001$.

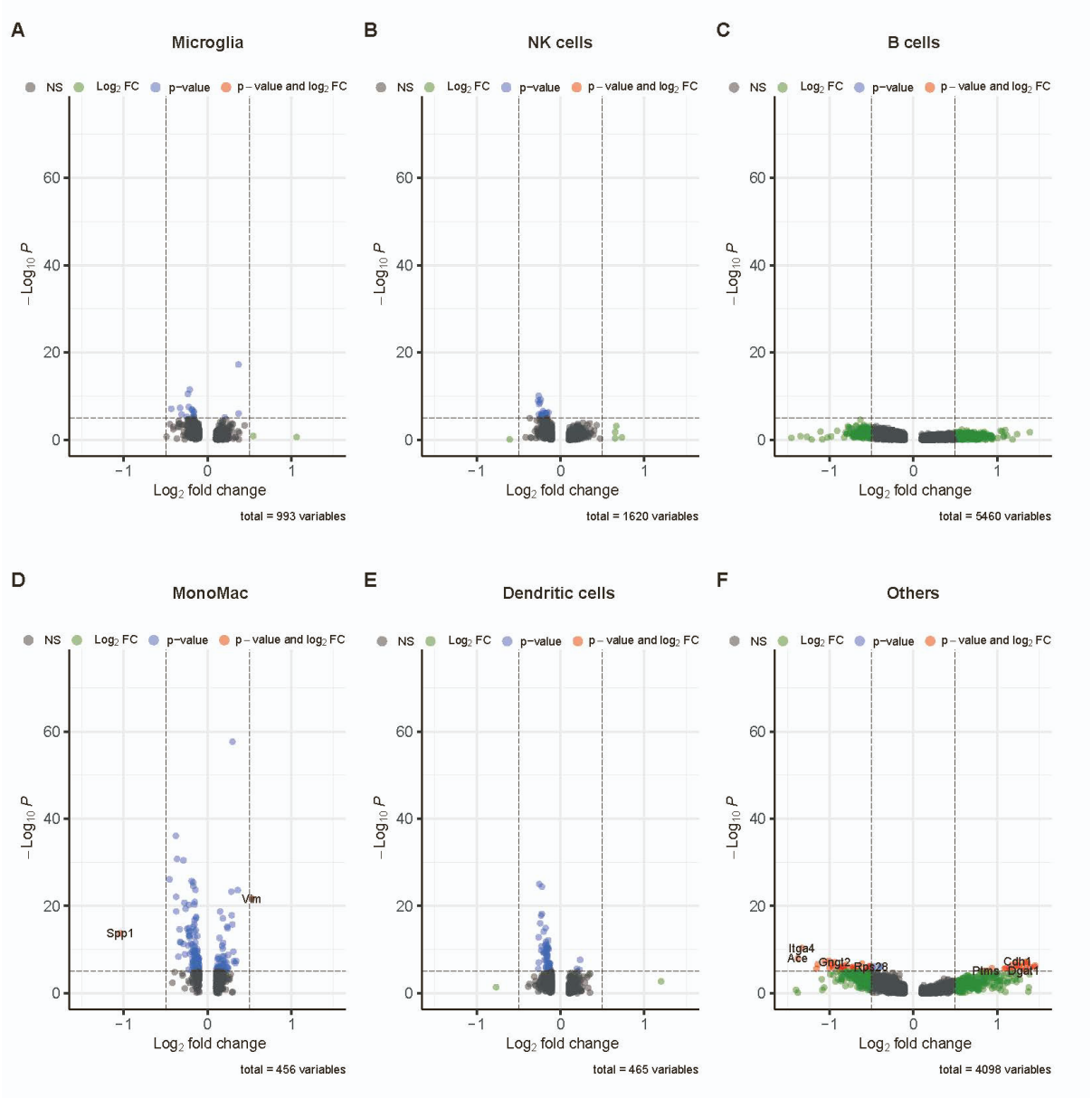

Figure S2. Volcano plot of differentially expressed genes for various immune cell types in the GBM tumor microenvironment, comparing the effects of CD vs. HGD supplementation, Related to Figure 2.

We performed single-cell RNA sequencing (scRNA-seq) analysis of mouse CD45.2^{+} immune cells in the GBM tumor microenvironment (TME) for immune cell profiling.

(A–F) Volcano plot of each immune cell cluster. Each dot represents one gene, and the $\log_2$ fold change indicates changes in mean gene expression level. Red dots represent genes that were significantly differentially expressed between CD and HGD groups. Dots on the right side indicate genes upregulated in the HGD group, and dots on the left side indicate genes upregulated in the CD group. (A) microglia, (B) natural killer (NK) cells, (C) B cells, (D) monocyte and macrophages (MonoMac), (E) dendritic cells, and (F) Others.

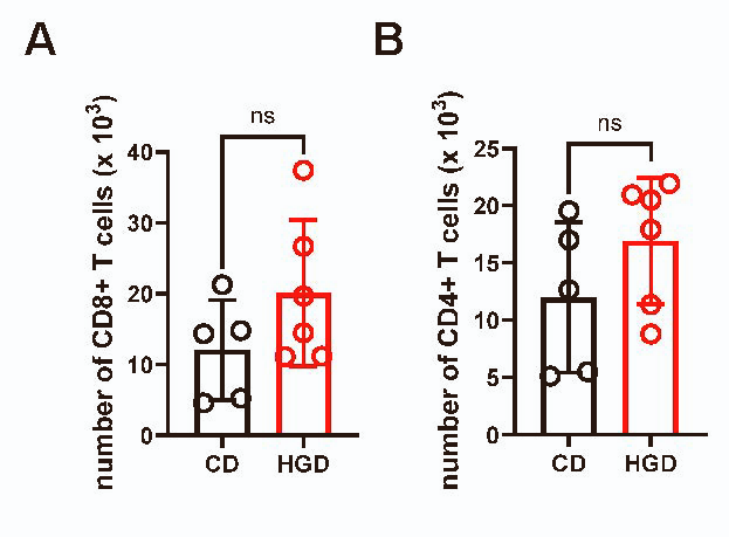

Figure S3. Analysis of the number of each T-cell subtype in the TME of the mouse GBM model by flow cytometry, Related to Figure 2.

Bar graph showing total number of $CD8^+$ T cells (A) and $CD4^+$ T cells (B) in the TME of the GL261 mouse GBM model in animals that received CD (n = 5) or HGD (n = 6) supplementation.

ns, not significant; $*p < 0.05$, $**p < 0.01$, $***p < 0.001$, $****p < 0.0001$.

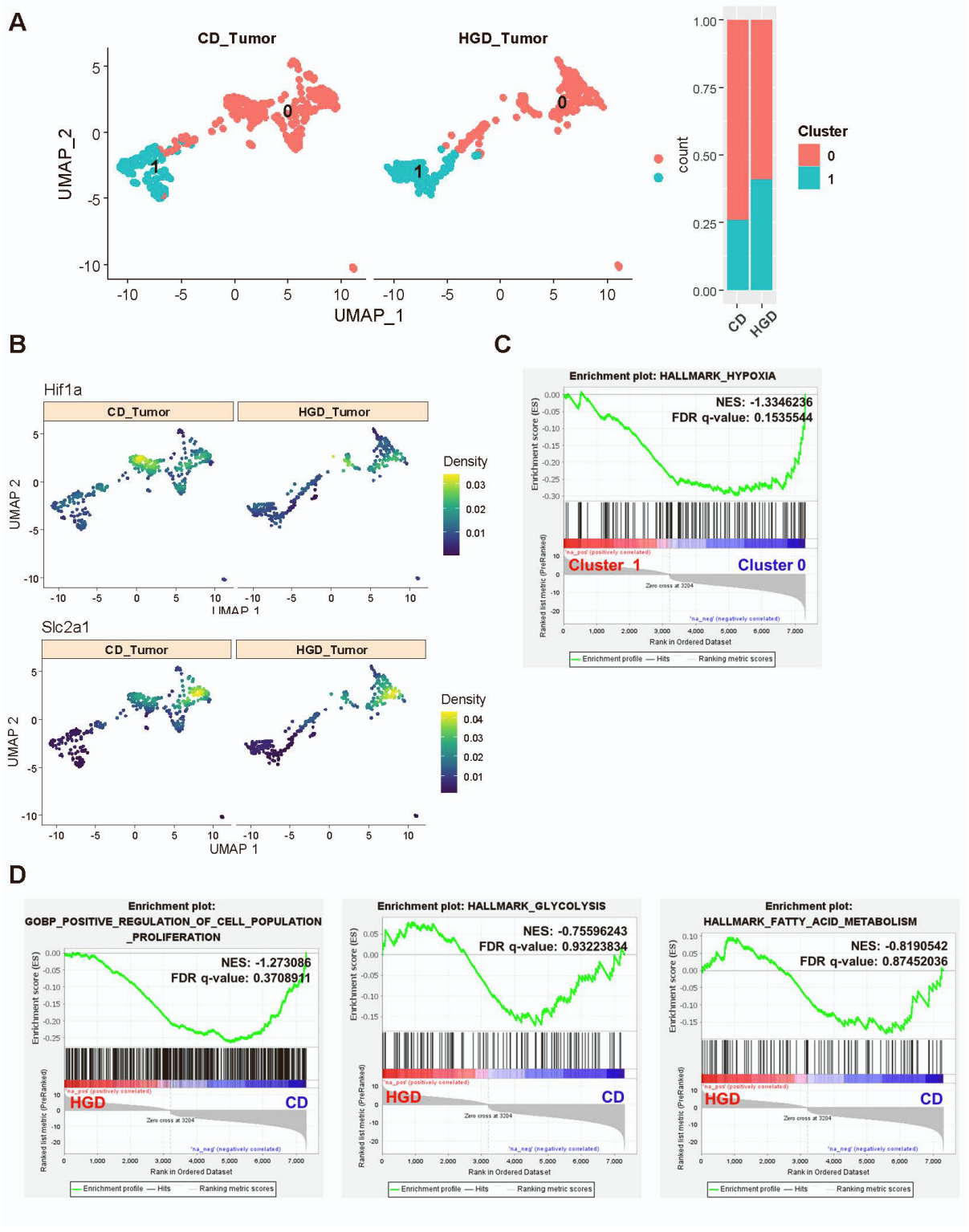

Figure S4. Single-cell RNA sequencing analysis of tumor cells showed that HGD supplementation did not directly affect tumor cells in terms of proliferative and metabolic changes, Related to Figure 2.

(A) UMAP of tumor cells between CD and HGD groups and the frequency of each cluster.

(B) Feature plot of *Hif1a* and *Slc2a1* gene expression levels in tumor cells between CD and HGD groups.

(C) Gene set enrichment analysis (GSEA) data regarding the differential expression of genes related to the HALLMARK_HYPOXIA gene set between cluster 0 and cluster 1. NES: normalized enrichment score, FDR: false discovery rate.

(D) GSEA data regarding the differential expression of genes related to the POSITIVE_REGULATION_OF_CELL_POPULATION_PROLIFERATION, HALLMARK_GLYCOLYSIS, and HALLMARK_FATTY_ACID_METABOLISM gene sets between the CD and HGD groups.

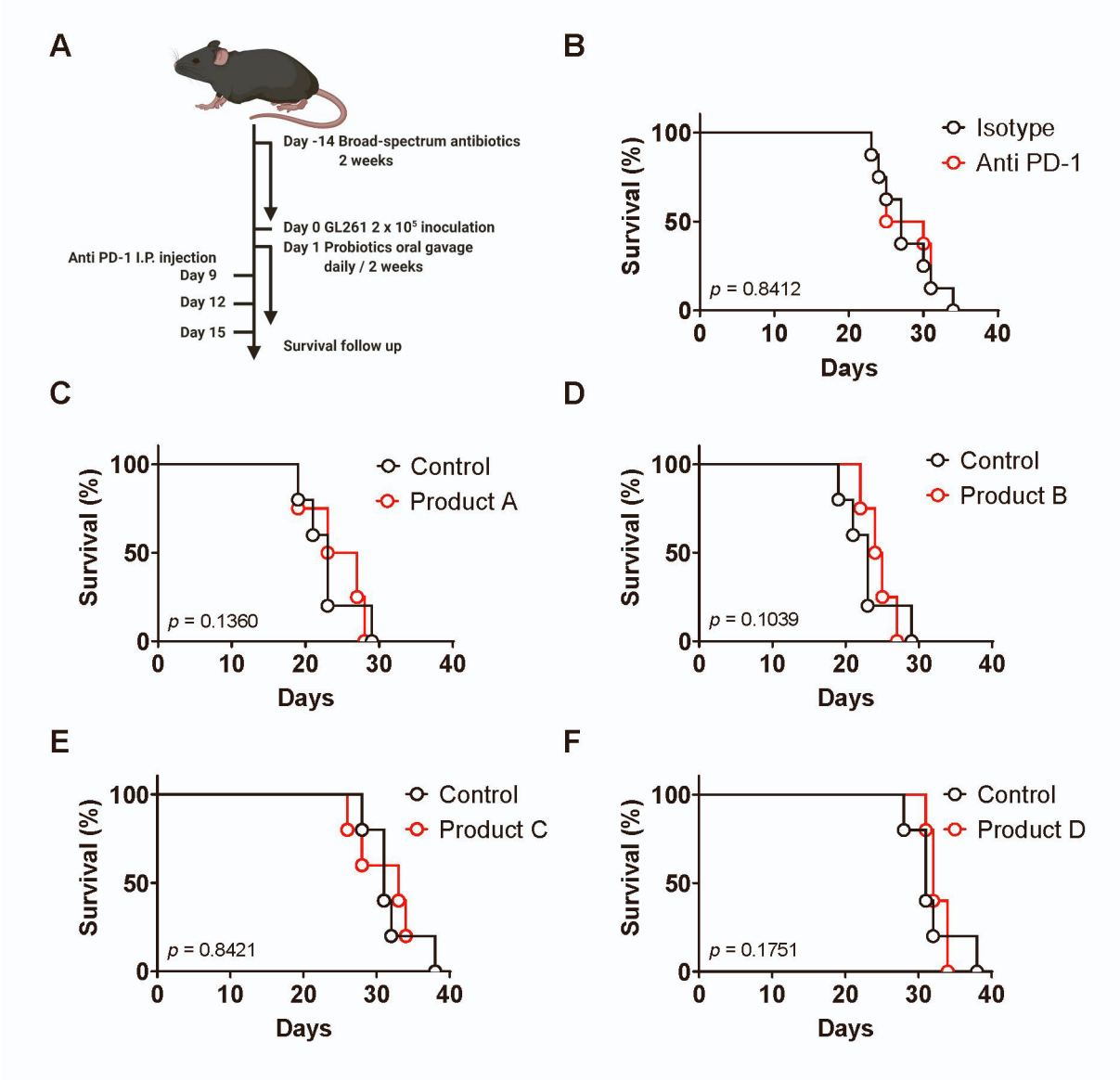

Figure S5. Commercial probiotics did not enhance the effect of the anti-PD-1 immune checkpoint blockade in GBM, Related to Figure 2.

(A) Schema for experiments to determine the effect of probiotics on the GL261 syngeneic GBM model mice. Survival rates were compared after oral gavage using each probiotic.

(B) Median survival of mice treated with isotype (27 days; n = 8) was compared with anti PD-1 (27.5 days; n = 8, p = 0.8412) in GL261 mouse glioma tumor cells by log-rank analysis.

(C–F) Median survival of GBM model mice treated with anti-PD-1 antibody and probiotics by log-rank analysis: (C) product A, CKD LACTO-FIT ProBiotics Gold (CKD, Korea) (23 days, n = 5 for control and 25 days, n = 4 for product A, p = 0.1360); (D) product B, CJ BYO Probiotics 2 Billion for Men (CJ Cheiljedang, Korea) (23 days, n = 5 for control and 24.5 days, n = 4 for product B, p = 1039); (E) product C, Denmark Probiotics Story (Denps, Denmark) (31 days, n = 5 for control and 33 days, n = 5 for product C, p = 8421); (F) product D, Esther

Formula Ultra Flora Probiotics Blue (Metagenics, Gig harbor, WA, USA) (31 days, n = 5 for control and 32 days, n = 4 for product D, p = 0.1751).

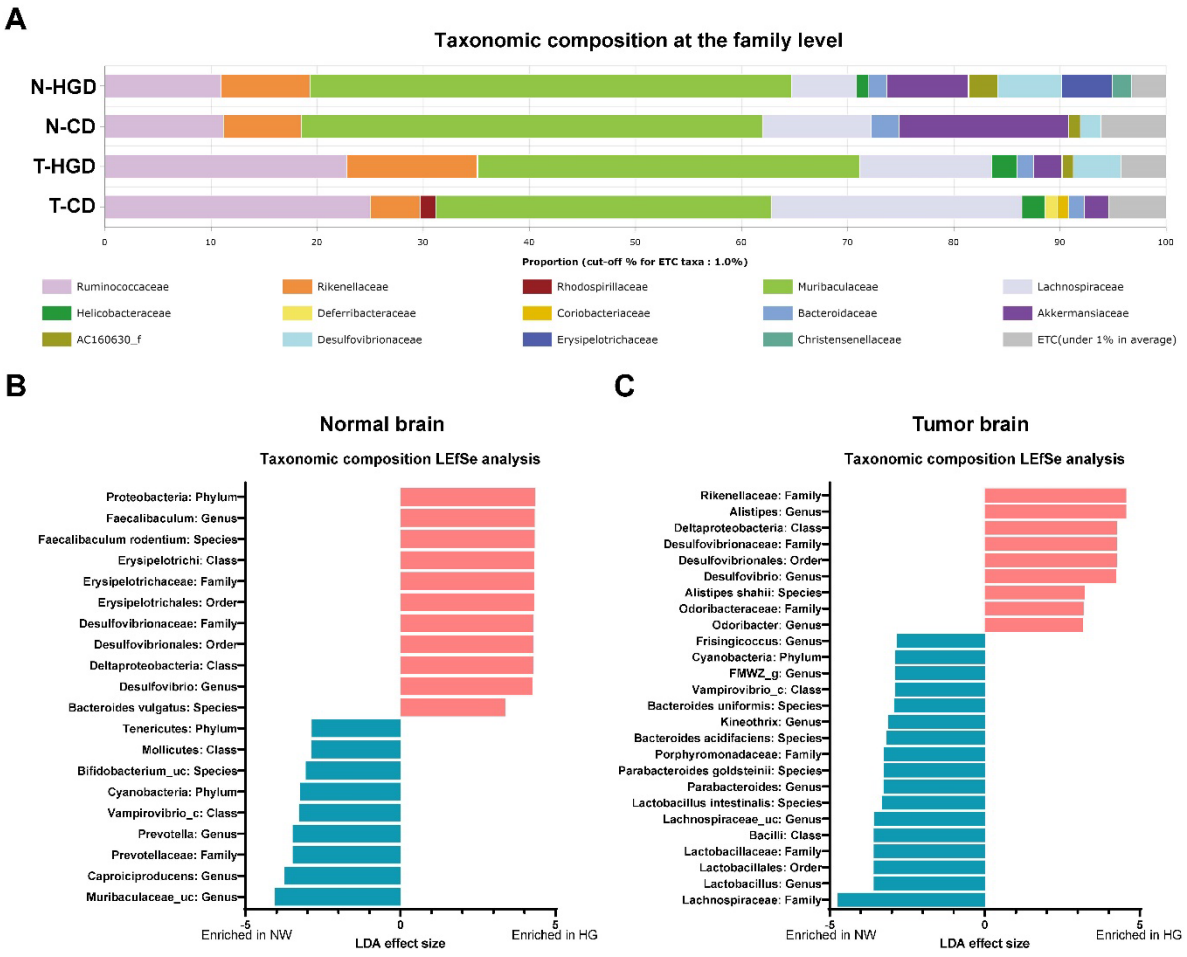

Figure S6. 16S rRNA gene sequencing revealed changes in the gut microbiota in mice fed an HGD in the presence or absence of a brain tumor, Related to Figure 4.

(A) Bar graph for the microbiota of each mouse group with the taxonomic composition at the family level based on 16S rRNA gene sequencing. N-CD, normal brain and control drink; N-HGD, normal brain and high-glucose drink; T-CD, tumor brain and control drink; T-HGD, tumor brain and high-glucose drink.

(B–C) Linear discriminant analysis (LDA) effect size analysis identified the most differentially abundant taxa of the gut microbiota for the CD vs. HGD groups (B) in normal brain and (C) in tumor brain. Unidentified taxa were excluded from this graph.

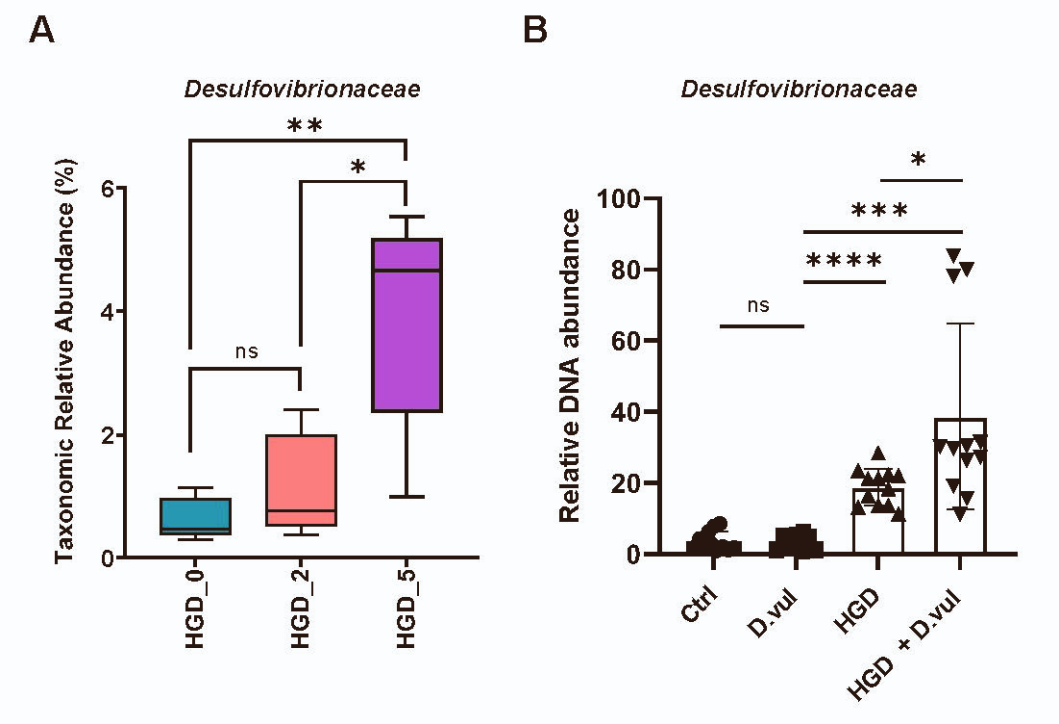

Figure S7. Gut colonization of the Desulfovibrionaceae strain with long-term HGD supplementation functioned as an essential factor for gut colonization of Desulfovibrionaceae strain, Related to Figure 4.

(A) Relative taxonomic abundance of the Desulfovibrionaceae family by group, as determined from 16S ribosomal RNA sequencing data: HGD_0, HGD supplementation was not implemented; HGD_2, HGD supplementation was continued for 2 weeks; HGD_5, HGD supplementation was continued for 5 weeks (n = 5 per group).

(B) Real-time quantitative PCR analysis of DNA abundance of the Desulfovibrionaceae family in fecal samples from each group. Ctrl (n = 11), CD with DPBS oral gavage; D.vul (n = 12), CD with *Desulfovibrio vulgaris* oral gavage; HGD (n = 12), HGD with DPBS oral gavage; HGD + D.vul (n = 12), HGD with *Desulfovibrio vulgaris* oral gavage.

ns, not significant; $*p < 0.05$, $**p < 0.01$, $***p < 0.001$, $****p < 0.0001$.

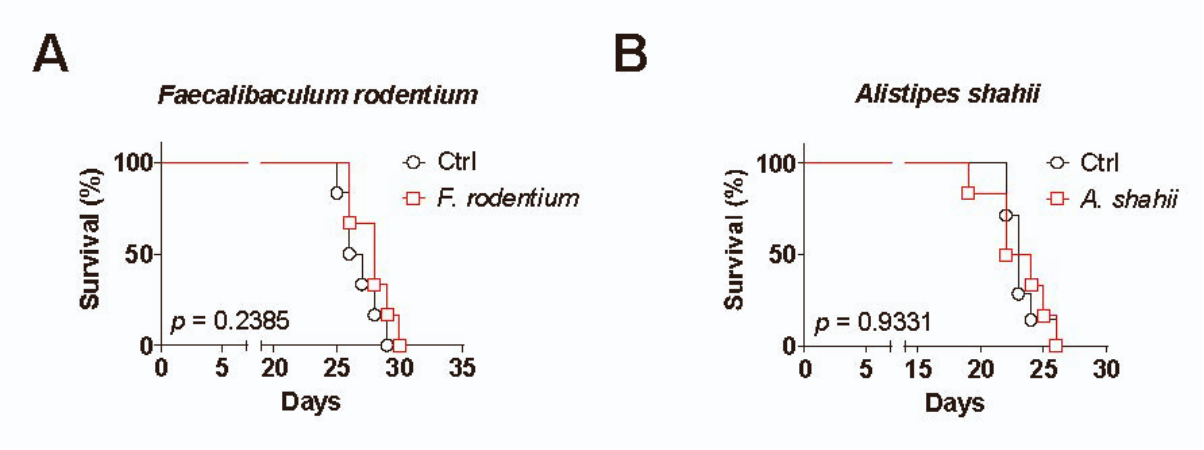

Figure S8. Other bacterial strains upregulated by HGD supplementation did not improve survival outcomes in the GL261 mouse GBM model, Related to Figure 4.

Median survival in GBM mice model with HGD supplement (A) treated with *Faecalibaculum rodentium* by oral gavage (28 days, n = 6) compared with DPBS oral gavage control (26.5 days, n = 6, p = 0.2385) or (B) treated with *Alistipes shahii* by oral gavage (23 days, n = 6) compared with DPBS oral gavage control (23 days, n = 7, p = 0.9331) after antibiotics treatment.

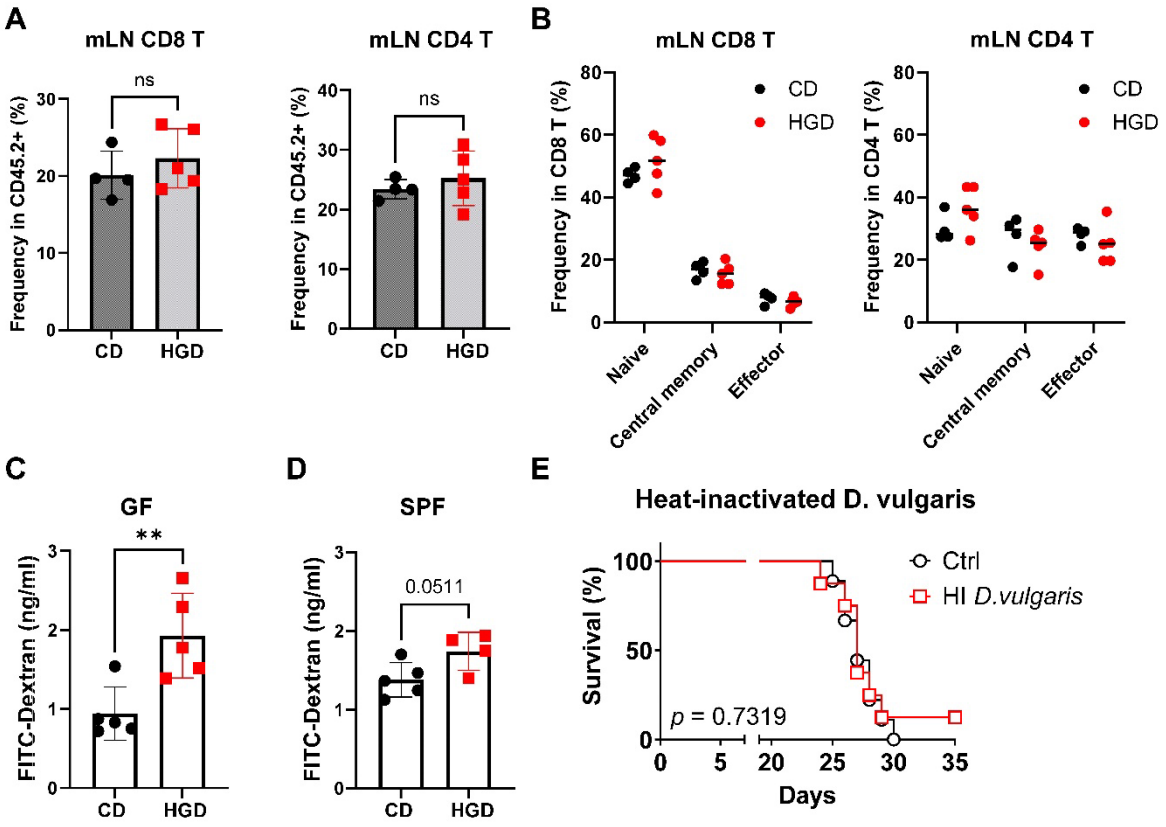

Figure S9. Identification of the impact of HGD supplementation on the gut environment, Related to Figure 4.

(A) Comparison of the frequencies of $CD8^+$ and $CD4^+$ T cells among $CD45.2^+$ immune cells in the mesenteric lymph nodes (mLN) between the CD (n = 4) and HGD (n = 5) groups.

(B) Analysis of each frequency of $CD8^+$ and $CD4^+$ T-cell subtypes (naïve T cells: $CD62L^+CD44^-$ T cells, central memory T cells: $CD62L^+CD44^+$ T cells, effector memory T cells: $CD62L^-CD44^+$ T cells) in the mLNs between the CD (n = 4) and HGD (n = 5) groups.

(C) Gut permeability test measuring the presence of 4-kDa fluorescein isothiocyanate-conjugated (FITC) dextran in the blood from tail vein samples taken 4 hours after the oral administration of dextran in (C) GF mice and (D) SPF mice (n = 5 per group).

(E) Median survival of mice administered with heat-inactivated (HI) *Desulfovibrio vulgaris* oral gavage (27 days, n = 8) compared with DPBS oral gavage control (27 days, n = 9, p = 0.7319) after administration of antibiotics to mice that had been fully supplemented with the HGD.

ns: not significant, * $p < 0.05$, ** $p < 0.01$.

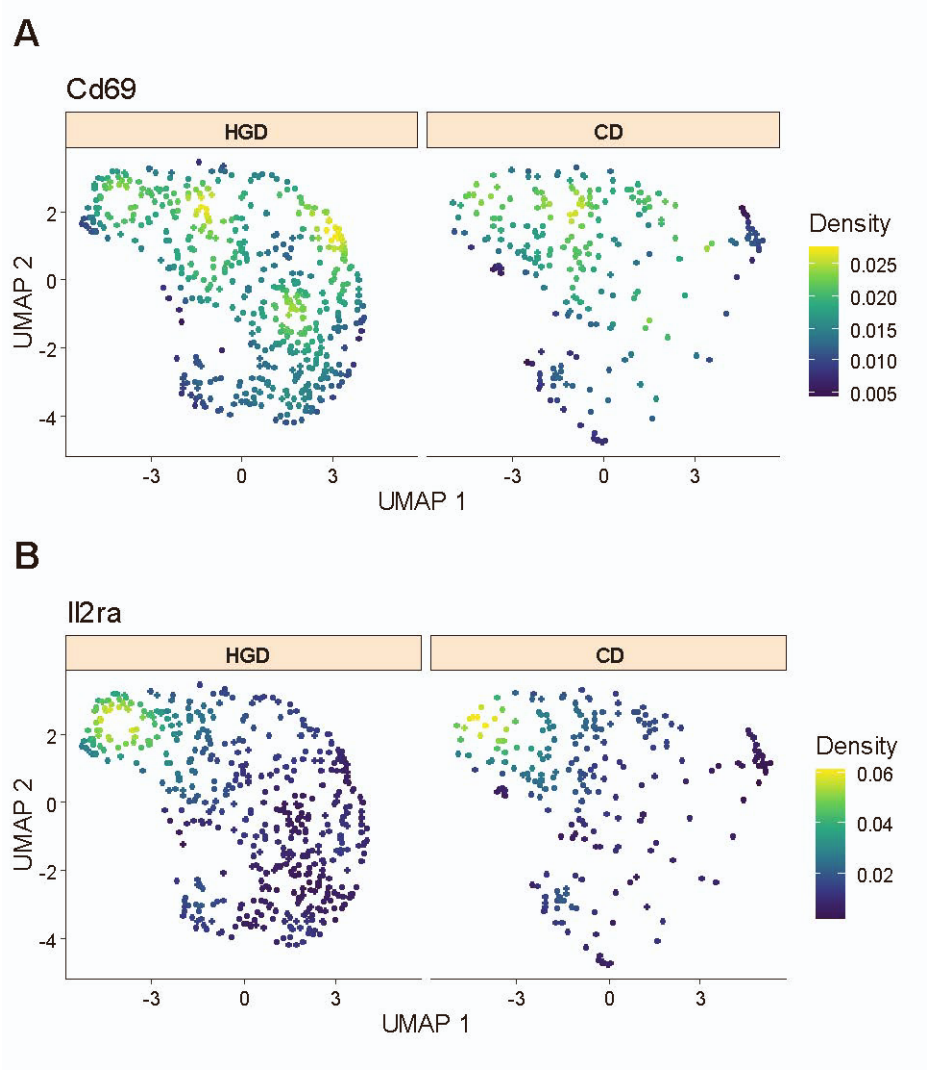

Figure S10. Comparison of activation markers between the CD and HGD groups in CD8$^+$ T cells in the TME of the mouse GBM model, Related to Figure 5.

Single-cell RNA sequencing data were used to analyze the activation markers in CD8$^+$ T cells between the CD and HGD groups. The feature plots represent the expression levels of the genes (A) *Cd69* and (B) *Il2ra*.

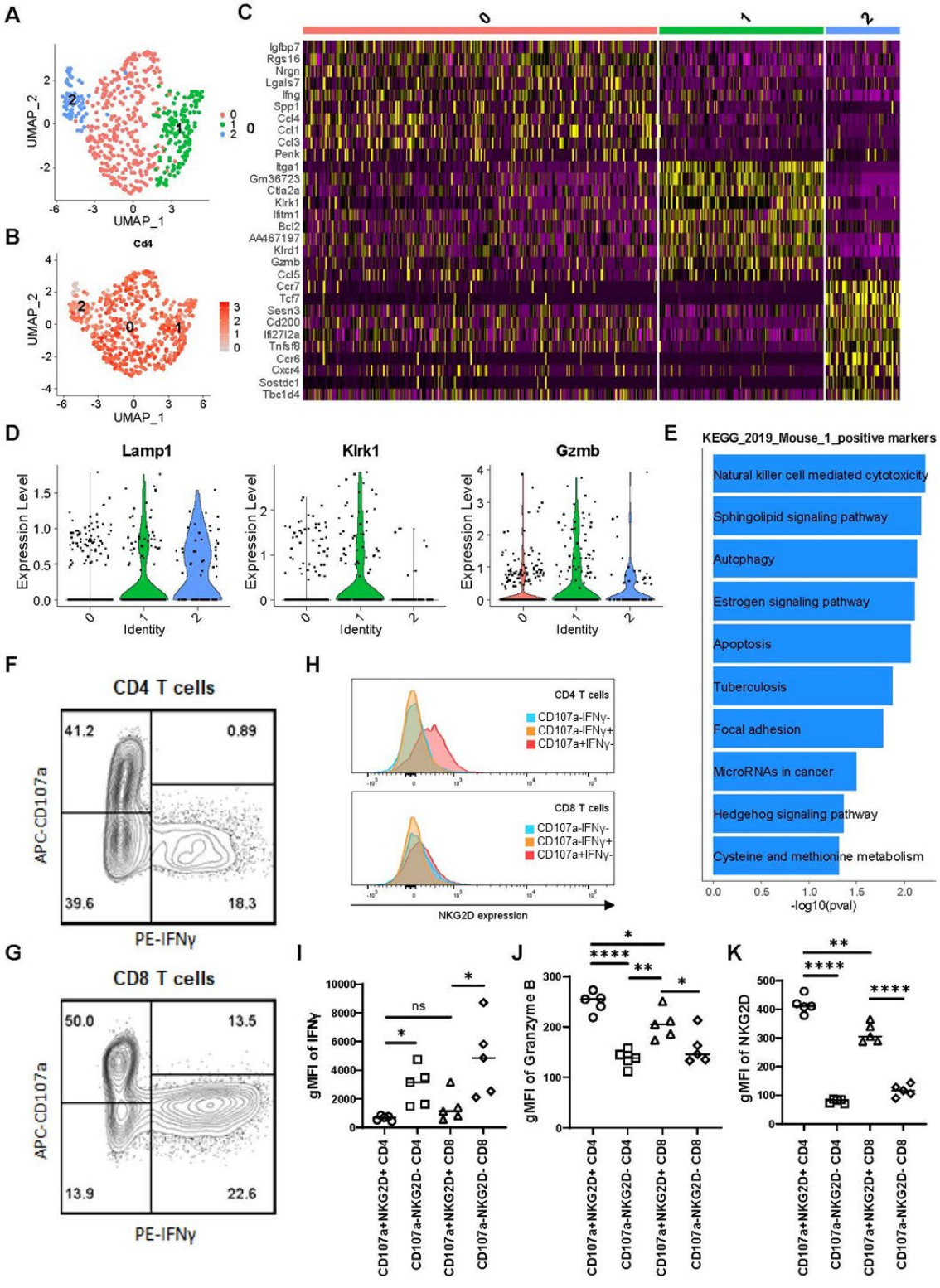

Figure S11. CD107a$^+$ NKG2D$^+$ cytotoxic CD4$^+$ T cells in the mouse GBM TME, Related to Figure 5.

(A–B) Uniform Manifold Approximation and Projection (UMAP) analysis of the $CD4^+$ T cell subcluster in the GBM TME. (A) $CD4^+$ T cells fell into three clusters. (B) All clusters exhibited high *Cd4* mRNA expression levels in a feature plot.

(C) Heatmap analysis of the 10 most highly expressed genes for each cluster.

(D) Violin plot of *Lamp1, Klrk1*, and *Gzmb* mRNA expression in each cluster.

(E) Functional enrichment analysis of differentially expressed genes (DEGs) in cluster 1 using enrichR and the Kyoto Encyclopedia of Genes and Genomes (KEGG) 2019 mouse database.

(F–G) Representative plot of the fluorescence-activated cell sorting (FACS) analysis of (F) $CD4^+$ and (G) $CD8^+$ T cells expressing CD107a and interferon (IFN)-γ. Immune cells were analyzed by gating on cells expressing CD4 or CD8 among $singlet^+$ fixable $viability^-$ $CD45.2^+$ immune cells.

(H) Representative histogram of NKG2D expression levels in cells constituting each quadrant in (F).

(I–K) Differences in geometric mean fluorescence intensity (gMFI) of (I) IFN-γ, (J) granzyme B, and (K) NKG2D expression in the subsets of $CD4^+$ and $CD8^+$ T cells according to CD107a expression (n = 5 per group). ns: not significant, * $p < 0.05$, ** $p < 0.01$, *** $p < 0.001$, and **** $p < 0.0001$.